EQUIVALENT EXCITABILITY THROUGH DIFFERENT SODIUM CHANNELS AND IMPLICATIONS FOR THE ANALGESIC EFFICACY OF SELECTIVE DRUGS

Yu-Feng Xie[1], Jane Yang[1,2], Stéphanie Ratté[1], Steven A. Prescott[1,2,3]*

[1]Neurosciences and Mental Health, The Hospital for Sick Children, Toronto, ON, Canada
[2]Institute of Biomedical Engineering, University of Toronto, Toronto, ON, Canada
[3]Department of Physiology, University of Toronto, Toronto, ON, Canada

***Corresponding Author:** Steven A. Prescott (steve.prescott@sickkids.ca)

Short Title: Implications of nociceptor degeneracy

ABSTRACT

Nociceptive sensory neurons convey pain-related signals to the CNS using action potentials. Loss-of-function mutations in the voltage-gated sodium channel $Na_V1.7$ cause insensitivity to pain (presumably by reducing nociceptor excitability) but efforts to treat pain by inhibiting $Na_V1.7$ pharmacologically have largely failed. This may reflect the variable contribution of $Na_V1.7$ to nociceptor excitability. Contrary to claims that $Na_V1.7$ is necessary for nociceptors to initiate action potentials, we show that nociceptors can achieve equivalent excitability using different combinations of $Na_V1.3$, $Na_V1.7$, and $Na_V1.8$. Selectively blocking one of those Na_V subtypes reduces nociceptor excitability only if the other two subtypes are weakly expressed. For example, excitability relies on $Na_V1.8$ in acutely dissociated nociceptors but responsibility shifts to $Na_V1.7$ and $Na_V1.3$ by the fourth day in culture. A similar shift in Na_V dependence occurs in vivo after inflammation, impacting ability of the $Na_V1.7$-selective inhibitor PF-05089771 to reduce pain in behavioral tests. Flexible use of different Na_V subtypes exemplifies degeneracy – equivalent function using different components – and compromises the reliable modulation of nociceptor excitability by subtype-selective inhibitors. Identifying the dominant Na_V subtype to predict drug efficacy is not trivial. Degeneracy at the cellular level must be considered when choosing drug targets at the molecular level.

SIGNIFICANCE STATEMENT

Nociceptors can achieve equivalent excitability using different sodium channel subtypes. The analgesic efficacy of subtype-selective drugs hinges on which subtype controls excitability. This contingency likely contributes to poor clinical outcomes.

INTRODUCTION

Chronic pain affects between 11 and 40% of the population worldwide (1). Neuropathic pain, which is pain arising from damage to the somatosensory nervous system, is particularly hard to treat with only 30% of patients achieving moderate (≥30%) relief using available treatments (2, 3). New treatments are needed but a meagre 11% of analgesic drugs entering phase 1 trials are ultimately approved (4), triggering debate about why basic science discoveries are not yielding improved clinical outcomes (5). Suggested explanations include flaws in preclinical animal testing (6, 7) or clinical trial design (8) but biological explanations must also be considered. For example, degeneracy – the ability of a biological system to achieve equivalent function using different components (9) – complicates modulation of neuronal excitability by allowing changes in diverse ion channels to potentially subvert the therapeutic effect of a drug targeting a particular channel (10). These explanations are not mutually exclusive but degeneracy continues to receive little consideration.

Like most neurons, nociceptive sensory neurons (nociceptors) rely on spikes to transmit information. Their excitability is thus critical for relaying information to the CNS. Nociceptor excitability is increased in many pathological pain conditions and the resultant increase in afferent input drives chronic pain (11-13). Neuronal excitability depends on the complex interplay between diverse ion channels (14-16) but some channels seem to be particularly important for pain. For instance, loss- or gain-of-function mutations in the gene *SCN9A*, which encodes the voltage-gated sodium channel $Na_V1.7$, cause congenital insensitivity to pain (CIP) or painful neuropathies, respectively (17-19); for review see (20). In rodents, nociceptor-specific deletion of $Na_V1.7$ abolishes acute and inflammatory pain (21) but not neuropathic pain (22, 23). Neuropathic pain is blocked by deleting $Na_V1.7$ globally, including from sympathetic neurons (24, 25), though not if the deletion is induced in adulthood (26). Furthermore, loss-of-function mutations in $Na_V1.7$ do not consistently reduce nociceptor excitability (see Discussion) and the associated insensitivity to pain involves increased opioid signaling (27, 28), consistent with naloxone's ability to restore pain sensitivity in CIP patients (27, 29). These observations cast doubt on whether $Na_V1.7$ mutations produce CIP by reducing nociceptor excitability, pointing instead to a less direct mechanism that may be harder to reproduce pharmacologically.

Notwithstanding such reservations, several $Na_V1.7$-selective drugs have been developed (30-32) but none

have yet passed phase 2 clinical trials (33-36). This has been attributed to poor target engagement (35, 37-39) yet prevention of the flare response by PF-05198007, a $Na_V1.7$-selective inhibitor, argues that at least some $Na_V1.7$ channels are blocked (40). But CIP patients exhibit a normal flare response (41), suggesting that their C fibers compensate for chronic loss of $Na_V1.7$ channels. Other $Na_V1.7$-selective inhibitors have struggled in phase 1 trials because of autonomic side effects (e.g. (42)), as might be expected if those drugs block $Na_V1.7$ channels on sympathetic neurons, which is apparently necessary to prevent/reverse neuropathic pain (see above). But CIP patients exhibit normal autonomic function (17, 41), suggesting that their sympathetic neurons also compensate for chronic loss of $Na_V1.7$ channels. In those patients, might similar compensation occur in nociceptors and restore pain, only for that effect to be masked by enhanced opioid signaling (see above)? Descriptions of $Na_V1.7$ as "the" threshold channel imply that it is irreplaceable for nociceptor excitability, consistent on the surface with pain insensitivity due to loss-of-function mutations in $Na_V1.7$ but inconsistent with some past electrophysiological data (43, 44). Clarifying whether nociceptors rely on $Na_V1.7$ is an unresolved issue important for predicting the analgesic efficacy of $Na_V1.7$-selective inhibitors.

A serendipitous observation prompted us to reassess the role of $Na_V1.7$ in nociceptor excitability and the implications for drug efficacy. Specifically, we observed that tetrodotoxin (TTX), which inhibits $Na_V1.7$ and several other TTX-sensitive (TTX-S) sodium channels, had variable effects in nociceptors, dramatically reducing their excitability in some conditions but not in others. This variability reveals that nociceptors can achieve equivalent excitability using different sodium channel subtypes, some of which are TTX-resistant (TTX-R). We demonstrate that a $Na_V1.7$-selective inhibitor produces analgesia only when nociceptor excitability relies on $Na_V1.7$. Insofar as increasingly selective drugs are more likely to have their efficacy subverted by degeneracy, our results have profound yet underappreciated implications for target selection and drug development.

RESULTS

Equivalent excitability can arise from different voltage-gated sodium (Na_V) channel subtypes

Small dorsal root ganglion (DRG) neurons (soma diameter <25 µm) tend to spike repetitively when depolarized by current injection (45). In our sample, most small neurons genetically identified as nociceptors (see Methods) spiked repetitively when tested 2-8 hours after dissociation (DIV0) or after 4-7 days

in culture (DIV4-7), though the proportion of repetitively spiking neurons increased slightly over that interval (χ^2=4.51, p=0.034, chi-square test) (**Fig. 1A**). Strikingly, 100 nM TTX had no effect on the spiking pattern at DIV0 but converted all but one neuron to transient spiking at DIV4-7. Amongst neurons that spiked repetitively at baseline, TTX reduced the firing rate and increased rheobase only at DIV4-7 (**Fig. 1B**). TTX reduced spike height at DIV0 and DIV4-7, but more so at DIV4-7. There was a significant increase in capacitance and leak conductance density between DIV0 and DIV4-7, but no change in resting membrane potential (**Fig. 1C**). Normalizing leak conductance by capacitance (which increases over time because of neurite growth) disambiguates whether changes in input resistance reflect changes in cell size or membrane leakiness. Consistent with current clamp data, voltage clamp recordings showed that only a small fraction of sodium current is TTX-S at DIV0, whereas nearly all sodium current was blocked by TTX at DIV4-7 (**Fig. 1D**). Previous studies suggested that TTX-R channels play an important role in nociceptor excitability (46-48). Our initial results confirm this for DIV0 but show that their contribution diminishes after a few days in culture, with TTX-S channels becoming dominant by DIV4. Despite this reconfiguring of Na_V channels, excitability was remarkably stable, consistent with previous work showing little change in excitability after axotomy despite large (but evidently counterbalanced) changes in TTX-R and TTX-S currents (43, 49). We show later that similar changes develop in vivo following inflammation with consequences for drug efficacy assessed behaviorally (see Fig. 8), suggesting the Na_V channel reconfiguration described above is not a trivial epiphenomenon of culturing.

Different Na_V channel subtypes control nociceptor excitability at DIV0 and DIV4-7

Next, we sought to identify the Na_V subtype responsible for repetitive spiking at each time point, starting with DIV0. Of the TTX-R Na_V channels expressed by nociceptors, $Na_V1.8$ has been implicated in repetitive spiking (47, 48). We measured sodium current in voltage clamp before and after applying the $Na_V1.8$-selective inhibitor PF-01247324 (PF-24) (50). At DIV0, 1 µM PF-24 abolished most of the sodium current (**Fig. 2A**). The PF-24-sensitive current had slow inactivation kinetics, like the TTX-R current and unlike the fast TTX-S current in Figure 1D, and consistent with previous descriptions of $Na_V1.8$ (51). A different $Na_v1.8$ antagonist, A-803467, had similar effects (**Fig. 2 – figure supplement 1**). In current clamp, PF-24 converted

7 of 8 repetitively spiking neurons to transient spiking and significantly reduced evoked spiking (**Fig. 2B**). It also increased rheobase and decreased spike height but did not affect resting membrane potential (**Fig. 2C**). PF-24 had negligible effects when tested at DIV4-7 (**Fig. 2 – figure supplement 2**). These results show that $Na_V1.8$ is the predominant Na_V subtype at DIV0 and is necessary for repetitive spiking at that time point. To test the sufficiency of $Na_V1.8$ to produce repetitive spiking, we tuned a single-compartment, conductance-based model neuron (see Methods) to reproduce DIV0 data described above. In this DIV0 model, inclusion of $Na_V1.8$ conductance was sufficient to generate repetitive spiking (**Fig. 2D** left). The necessity of $Na_V1.8$ for repetitive spiking at DIV0 was also recapitulated: 85% reduction in the $Na_V1.8$ conductance converted spiking from repetitive to transient (**Fig. 2D** and **Supplementary Table 1**).

Next, we sought to identify the Na_V subtype responsible for repetitive spiking at DIV4-7 using PF-05089771 (PF-71) to inhibit $Na_V1.7$ (40, 52) and ICA-121431 (ICA) to inhibit $Na_V1.1/1.3$ (53, 54). Since $Na_V1.1$ is expressed mostly in medium-diameter (Aδ) neurons (55) whereas $Na_V1.3$ is known to be upregulated in C fibers after injury (for review, see 56), we ascribe the ICA effect to blockade of $Na_V1.3$. In voltage clamp, sodium current was significantly reduced by 30 nM PF-71, and most of the remaining current was blocked by 1 μM ICA (**Fig. 3A**). In current clamp, each inhibitor (applied separately) converted a significant proportion of neurons to transient spiking and significantly reduced firing rate (**Fig. 3B**). This argues that $Na_V1.7$ and $Na_V1.3$ are both necessary for repetitive spiking at DIV4-7. Inhibiting $Na_V1.7$ increased rheobase, unlike inhibiting $Na_V1.3$, and caused a stronger reduction in spike height (**Fig. 3C**). Neither affected resting membrane potential. These results show that $Na_V1.7$ is the predominant Na_V subtype at DIV4-7, but not the only one. PF-71 had negligible effects when tested at DIV0 (**Fig. 3 – figure supplement 1)**. We re-tuned our computational model to reproduce DIV4-7 data, with both $Na_V1.7$ and $Na_V1.3$ being required to produce repetitive spiking, meaning neither channel is individually sufficient (**Fig. 3D** and **Supplementary Table 1**). That said, inserting a higher density of either $Na_V1.7$ or $Na_V1.3$ could produce repetitive spiking in the absence of the other subtype (**Fig. 3 – figure supplement 2)**, consistent with $Na_V1.7$ and $Na_V1.3$ also being interchangeable.

Acutely interchanging Na_V subtypes does not affect spiking pattern

The ability of $Na_V1.3$, $Na_V1.7$ and $Na_V1.8$ to each encourage repetitive spiking is seemingly inconsistent with the common view that each Na_V subtype contributes selectively to a different phase of the spike (for example, Figure 3 in ref. 56). If $Na_V1.8$ were to activate exclusively at suprathreshold voltages, it could not initiate spikes and a different perithreshold-activating Na_V channel would be needed, which is clearly inconsistent with our data. To verify that $Na_V1.7$ and $Na_V1.8$ currents are each sufficient to produce repetitive spiking, we tested whether the $Na_V1.8$ current necessary for spiking in our DIV0 computer model could be replaced with $Na_V1.7$, and whether the $Na_V1.7$ current necessary for spiking in our DIV4-7 computer model could be replaced with $Na_V1.8$. In both cases, repetitive spiking was restored after inserting the alternate current (**Fig. 4A**). We then proceeded with equivalent experiments in real neurons, inhibiting $Na_V1.8$ with PF-24 on DIV0 or $Na_V1.7$ with PF-71 on DIV4-7, and then introducing the alternate channel virtually using dynamic clamp (see *Methods*). The replacement was successful in all neurons tested (**Fig. 4B**). Inserting virtual $Na_V1.8$ after inhibiting native $Na_V1.8$ also restored repetitive spiking, and likewise for $Na_V1.7$ (**Fig. 4 – figure supplement 1**), verifying that our virtual channels were equivalent to the native channels we aimed to replace. Apart from maximal conductance density, which was titrated in each neuron, all other parameters used for dynamic clamp were identical to simulations. The success of dynamic clamp experiments helps validate our computational models insofar as virtual $Na_V1.7$ and $Na_V1.8$ currents interacted appropriately with native currents to produce repetitive spiking in real neurons, the same way they interact with other simulated currents in the model neuron. Please note that tests reported In **Figure 4B** involve replacing a native channel with a different virtual channel (e.g. native $Na_V1.8$ replaced with virtual $Na_V1.7$) whereas tests reported in **Figure 4 – figure supplement 1** involve replacing a native channel with the equivalent virtual channel (e.g. native $Na_V1.8$ replaced with virtual $Na_V1.8$); the former demonstrates that Na_V subtypes are interchangeable whereas the latter serves as a positive control.

With the model neurons thus validated, we used simulations to infer $Na_V1.7$ and $Na_V1.8$ currents during different phases of the spike (**Fig. 5A-D**). Since inward (depolarizing) current at voltages just below spike threshold is critical for spike initiation (57), we sought to identify which Na_V contributes to the subthreshold

current. In the DIV0 model (**Fig. 5A,B**), subthreshold inward current was mediated mostly by $Na_V1.7$ during the first spike (left) but by $Na_V1.8$ during the second and all subsequent spikes (right). We interpret this to mean that the first spike is initiated using $Na_V1.7$ whereas all subsequent spikes are initiated using $Na_V1.8$. This is explained by the small $Na_V1.7$ conductance at DIV0 quickly inactivating during the first spike and remaining inactive during subsequent spikes (**Fig. 5 – figure supplement 1A**). This is consistent with experimental results, where repetitive spiking at DIV0 was unaffected by inhibiting $Na_V1.7$ (see Fig. 1 and Fig. 3 – figure supplement 1) but was prevented by inhibiting $Na_V1.8$ (see Fig. 2). Inactivation of $Na_V1.7$ after the first spike was reflected by an increase in voltage threshold between the first and second spike in the model (**Fig. 5A**), which prompted us to check if the same increase was evident experimentally, which it was (**Fig. 5E**). This unanticipated simulation result also predicted that TTX should affect the voltage threshold of the first spike in DIV0 neurons despite not having other notable effects (see Fig. 1); as predicted, TTX caused a significant depolarizing shift in voltage threshold at DIV0 (**Fig. 5 – figure supplement 2)**, further validating our model. In the DIV4-7 model **(Fig. 5C,D)**, subthreshold inward current was mediated by $Na_V1.7$ and $Na_V1.3$ during the first spike (left) and during all subsequent spikes (right), with $Na_V1.8$ contributing little. Even though inactivation reduced $Na_V1.7$ and $Na_V1.3$ current after the first spike (**Fig. 5 – figure supplement 1B)**, those channels nonetheless provided sufficient inward current to support repetitive spiking at DIV4-7. Inactivation at DIV4-7 was reflected, however, in a combination of higher threshold and lower spike overshoot for the second spike, both in the model (**Fig. 5C,D**) and in experiments (**Fig. 5E**).

These results demonstrate that each Na_V subtype does not contribute exclusively to a particular phase of the spike, and nor is each spike phase mediated exclusively by a particular Na_V subtype. Instead, each Na_V subtype contributes preferentially to a different spike phase depending on its voltage-dependency and on the conductance densities and inactivation status of other Na_V subtypes; for instance, $Na_V1.8$ is often said to activate only at suprathreshold voltages, during the upswing of the spike, after the spike is initiated by $Na_V1.7$; but if $Na_V1.7$ is absent or inactivated, voltage threshold shifts into the $Na_V1.8$ activation range, thus enabling $Na_V1.8$ to activate at voltages that are now subthreshold. Indeed, a subtype's contribution can shift rapidly (because of channel inactivation) or slowly (because of changes in conductance density; see below).

Changes in Na_V subtype expression between DIV0 and DIV4-7

Next, we sought to identify the basis for the slow shift in which Na_V subtype controls nociceptor excitability. **Figure 6A** shows mRNA levels for $Na_V1.7$ and $Na_V1.8$ relative to a housekeeping gene (left) and to each other (right). $Na_V1.7$ mRNA levels exceeded $Na_V1.8$ mRNA levels at both DIV0 and DIV7. Both decreased between DIV0 and DIV7, but $Na_V1.8$ more so, resulting in a significant decrease in the $Na_V1.8$:$Na_V1.7$ mRNA ratio. This pattern is consistent with the reduced role of $Na_V1.8$ at DIV4-7 but is inconsistent with the negligible role of $Na_V1.7$ at DIV0; specifically, we expected $Na_V1.7$ mRNA levels to increase between DIV0 and DIV7. Next, we investigated if functional changes were better reflected by changes in protein levels. Immunofluorescence for $Na_V1.8$ was higher than for $Na_V1.7$ at DIV0, and that ratio reversed at DIV7 (**Fig. 6B**), consistent with functional changes. Moreover, cercosporamide (10 µM), a potent inhibitor of the eukaryotic translation Initiation Factor 4E (eIF4E), significantly mitigated the decrease in $Na_V1.8$ immunofluorescence and the increase in $Na_V1.7$ immunofluorescence when applied to cultured neurons for 24 or 120 hours prior to measurements on DIV5 (**Fig. 6C**). Beyond showing that their mRNA levels do not correlate well with Na_V contributions to nociceptor excitability, reminiscent of some previous work (e.g. (58)), these results suggest that translational regulation is crucial, though membrane trafficking and other downstream processes likely also contribute (59, 60). Specifically, our results suggest that there is not enough pre-existing $Na_V1.7$ channels that trafficking those channels to the membrane can explain observed functional changes; instead, synthesis of new $Na_V1.7$ protein from existing $Na_V1.7$ mRNA is involved, but that does not rule out changes in how $Na_V1.7$ protein is handled or why Nav1.8 decreases. Further investigation is required to explore those mechanisms.

Analgesic efficacy of subtype-selective drugs depends on which Na_V controls nociceptor excitability

If a $Na_V1.7$-selective inhibitor mediates analgesia by modulating nociceptor excitability, its analgesic efficacy hinges on nociceptor excitability being controlled by $Na_V1.7$. Accordingly, we predicted that the $Na_V1.7$-selective inhibitor PF-71 would have little if any effect on paw withdrawal under normal conditions, when $Na_V1.8$ controls nociceptor excitability (Fig. 2 and Fig. 3 – figure supplement 1), but would be effective if $Na_V1.7$ took over control. Inflammation increases $Na_V1.7$ channel trafficking and membrane expression

(61-64). To test if inflammation increased $Na_V1.7$'s influence on nociceptor excitability, we recorded neurons acutely dissociated (DIV0) from DRGs of mice whose hind paw was injected with CFA three days prior. Sample traces in Figure 7A show that inflammation caused nociceptors to become much more variable in their reliance of specific Na_V subtypes, presumably because neurons innervating the inflamed paw experience greater effects of inflammation than neurons innervating other, non-inflamed sites. Specifically, application of PF-71 to inhibit $Na_V1.7$ converted 5 of 12 (42%) CFA neurons to transient spiking vs 0 of 9 (0%) of control neurons, which is a significantly higher proportion ($p = 0.0451$, Fisher exact test, **Fig. 7B, left**), whereas subsequent application of PF-24 to inhibit $Na_V1.8$ converted only 1 of 7 (14%) of the remaining repetitive spiking CFA neurons to transient spiking vs 7 of 8 (88%) of control neurons, which is a significantly lower proportion ($p = 0.001$). PF-71 also significantly affected resting membrane potential, rheobase, and spike height after CFA (**Fig. 7C**), unlike in control neurons (see Fig. 3 – figure supplement 1).

Results above confirm that $Na_V1.7$ takes on greater responsibility for nociceptor excitability after inflammation, which in turn predicts that PF-71 should reduce pain after inflammation but not under control conditions. As predicted, PF-71 significantly reduced thermal (**Fig. 8A**) and tactile (**Fig. 8B**) sensitivity in CFA-inflamed mice without having any effect in control mice. These results show that the inflammation-induced shift in Na_V subtype expression, despite being variable (see Fig. 7), is sufficient to cause a measurable change in drug efficacy assessed in vivo. Consistent with this, epigenetic repression of $Na_V1.7$ prevents/reverses hypersensitivity in inflamed and neuropathic mice without causing hyposensitivity in naïve mice (65). This is unlike genetic deletion of $Na_V1.7$, which reduces thermal and tactile sensitivity in naïve mice (27), and with loss-of-function mutations in $Na_V1.7$ that abolish pain in humans (17). These inconsistencies rekindle concerns whether $Na_V1.7$ mutations, unlike pharmacological interventions, affect pain through mechanisms other than modulation of nociceptor excitability. Pharmacological reversal of hypersensitivity in chronic pain conditions (when $Na_V1.7$ is pathologically upregulated) without reducing normal nociceptive pain is clinically desirable, but this hinges on nociceptor hyperexcitability being $Na_V1.7$-dependent, which may be true of some but not all chronic pain conditions, or in only a subset of patients (66) (see Discussion).

DISCUSSION

Our results show that nociceptors can achieve similar excitability using different Na_V channels. Whereas repetitive spiking depends on $Na_V1.8$ shortly after dissociation (Fig. 2) and presumably under normal conditions in vivo, responsibility shifts to $Na_V1.7$ and $Na_V1.3$ after a few days in vitro (Fig. 3). This is due to translationally regulated changes in Na_V expression (Fig. 6). Inflammation causes a similar shift in vivo (Fig. 7). Importantly, acutely inhibiting a particular Na_V is consequential (analgesic) only if that subtype is responsible for nociceptor excitability (Fig. 8). This may explain why $Na_V1.7$-selective drugs have not performed well in clinical trials (see Introduction) – because $Na_V1.7$ is not always necessary for nociceptor excitability depending on the expression level of $Na_V1.7$ and other Na_V subtypes. Faster processes like channel inactivation also affect their relative contribution (Fig. 5). These observations demonstrate the variable contribution of different Na_V subtypes to nociceptor excitability. When unaccounted for, such variability can lead to inconsistencies at the root of poor reproducibility and translatability.

Although we have focussed here on Na_V channels, numerous other channels are likely to change during culturing and in response to subtler, more clinically relevant in vivo insults like inflammation. Those changes occur through diverse mechanisms. Our results argue that transcriptional changes in $Na_V1.7$ do not account for its upregulation between DIV0 and DIV4-7, but transcriptional changes in other genes might nonetheless be important. And though our data implicate translational regulation, much more work is needed to work out the details. That work should consider the other ion channels and associated proteins (e.g. beta subunits) that interact with Na_V channels, either physically or via mutual effects on membrane potential. In a degenerate system, one should ideally consider all the components contributing to the process of interest, but perfect is the enemy of good, which is to say that degeneracy should still be considered even with incomplete understanding of the system. Indeed, the interchangeability of Na_V subtypes demonstrated here may help explain why subtype-specific drugs are not reliably effective again pain, even if myriad other still unidentified changes are also taking place.

Contrary to the view that certain ion channels are uniquely responsible for certain aspects of neuronal function, neurons use diverse ion channel combinations to achieve similar function (67, 68). This

degeneracy is crucial for enabling excitability and other aspects of neuron physiology to be homeostatically regulated by adjusting ion channels in response to perturbations (69-71). Degeneracy also enables pathological changes in different ion channels to produce equivalent hyperexcitability (72). This is important insofar as similar excitability may belie differences in the underlying ion channels – differences that may render a neuron susceptible or impervious to a drug depending on the functional necessity of the targeted ion channel in that neuron. This is precisely what our data demonstrate in nociceptors. Similar observations have been made in substantia nigra neurons, whose pacemaker activity can be mediated by Na_V channels or by voltage-gated calcium channels, meaning TTX may or may not block their spiking (72, 73). Similar interchangeability is evident for the burst firing of Purkinje neurons (74).

Degeneracy also exists at the circuit level (75, 76), where it allows differences in the intrinsic excitability of component neurons to be offset (and effectively hidden) by differences in synaptic weights (77). Relevant for pain processing, the spinal dorsal horn circuit can achieve similar output using different synaptic weight combinations (78); specific neuron types may have a greater or lesser impact on circuit function depending on those weights. In effect, degeneracy introduces contingencies. The role of any ion channel in a neuron (or any neuron in a circuit) depends on the other ion channels in that neuron (or the synaptic connections with other neurons in the circuit). Because of such contingencies, a drug may engage its target without producing the intended cellular, circuit or clinical effect. Indeed, different combinations of $GABA_A$ receptor activation and chloride driving force can produce equivalent synaptic inhibition (79), but when inhibition is incompensably compromised, the underlying cause necessitates different interventions (80). By this logic, if upregulation of $Na_V1.7$ is responsible for nociceptor hyperexcitability after nerve injury or inflammation, $Na_V1.7$ is an ideal target since "normal" neurons (not reliant on $Na_V1.7$) would be spared the effects of a $Na_V1.7$-selective drug, but the long-term efficacy of such a drug hinges on hyperexcitability remaining $Na_V1.7$-dependent, which cannot be assumed (10). Furthermore, if myelinated afferents (which express minimal $Na_V1.7$ (81)) are responsible for mechanical allodynia under neuropathic conditions (82-85), then $Na_V1.7$-selective drugs should not be expected to alleviate that symptom, which evidently they do not (26), at least not through a direct mechanism. Indeed, ablating nociceptors abolishes acute and inflammatory pain

but not neuropathic pain (23, 86). Pathological pain being mediated by more than one afferent type is another example of circuit-level degeneracy.

To be interchangeable, Na_V subtypes must functionally overlap (87, 88). Indeed, $Na_V1.8$ and $Na_V1.7$ are similar but not identical in their gating properties; for example, their voltage-dependencies partially overlap but the activation curve for $Na_V1.8$ is right-shifted compared to $Na_V1.7$ (89). Consequently, $Na_V1.7$ activates at voltages near threshold whereas $Na_V1.8$ tends to activate at suprathreshold voltages, during initiation and upstroke of the spike, respectively (34, 56). But that separation is not absolute. We found that $Na_V1.7$ contributes to initiation of the first spike in DIV0 neurons, but because it inactivates more readily than $Na_V1.8$, initiation of all subsequent spikes depends on $Na_V1.8$ (see Fig. 5), which activates at perithreshold voltages because voltage threshold is high (depolarized) in the absence of $Na_V1.7$. At DIV4-7, $Na_V1.7$ still inactivates (which causes voltage threshold to rise) but, because of its higher density, continues to produce enough inward current to continue to initiate later spikes. The activation pattern we report for the first spike at DIV0 is consistent with Blair and Bean (90) who quantified the contribution of different Na_V channels by recording pharmacologically isolated currents while varying the holding potential according to the spike waveform. Our results go further in showing how responsibilities shift across different spikes within a train (because of differential Na_V inactivation) and across conditions (because of changes in Na_V expression). Although we focused on Na_V channels in this study, other ion channels are likely also undergoing changes; indeed, changes in the AHP shape between DIV0 and DIV 4-7 (see Figure 1A) point to changes in potassium channels. All neurons presumably regulate their excitability in a degenerate manner but likely do so by adjusting different sets of ion channels. Even within a given neuron type, the identify of adjusted ion channels may depend on the nature of the perturbation or on a multitude of other conditions.

With respect to reproducibility, labs testing nociceptors after different times in vitro would be expected to reach contradictory conclusions about the relative importance of a given Na_V subtype. Likewise, a testing protocol focusing on single spikes (the equivalent to the first spike in a train) would yield different results from one that considers repetitive spiking. Along the same lines, voltage clamp protocols that deliberately hold membrane potential at unnaturally hyperpolarized voltages to relieve inactivation before stepping up

the voltage can give a misleading impression of how much a Na_V subtypes contributes under natural conditions (i.e. with natural levels of inactivation). Such discrepancies might be chalked up to irreproducibility if the consequences of those methodological differences are not appreciated, especially if one overlooks how degeneracy allows responsibilities to shift between ion channels. Indeed, the pain literature is replete with apparent inconsistencies. We would argue that most of those studies are correct, but only under limited conditions. Failure to identify and report those conditions (contingencies) represents a huge impediment to translation. A recent review of degeneracy in epilepsy (91) reveals many similarities with chronic pain. Observations that effective antiseizure medications often act on multiple targets and that patients with the same type of epilepsy respond heterogeneosly to a given treatment offer circumstantial evidence of degeneracy, but more deliberate testing is required to quantify degeneracy and its impact.

In summary, our results show that nociceptors can achieve equivalent excitability using different Na_V subtypes. The importance of a given subtype can shift on long and short timescales, yielding results that are seemingly inconsistent. By elucidating those shifting responsibilities, our results highlight the degenerate nature of nociceptor excitability and its functional implications. Degeneracy makes it impossible to claim without reservation that a particular Na_V subtype is uniquely responsible for pathological pain. Greater appreciation of degeneracy's implications would prompt better experimental design, more cautious interpretation, and, ultimately, improved translation.

MATERIALS AND METHODS

Animals

All animal procedures were approved by the Animal Care Committee at The Hospital for Sick Children (protocol #53451) and were conducted in accordance with guidelines from the Canadian Council on Animal Care. We used the Cre-*lox*P recombinase system to generate mice that express ChR2-eYFP in Na_V1.8-expressing neurons. Mice were obtained by crossing homozygous Ai32 mice (B6.Cg-Gt(ROSA)26Sortm32(CAG-COP4*H134R/EYFP)Hze/J) from Jax (#012569), which express ChR2(H134R)-eYFP in the presence of Cre recombinase, with Na_V1.8-Cre mice (Tg(Scn10a-cre)1Rkun), which express Cre recombinase in Na_v1.8-expressing neurons (kindly provided by Rohini Kuner). These neurons are primarily

nociceptive and thermoreceptive (92). The $Na_V1.8$ promoter leads to transgene expression in >90% of neurons expressing markers of nociceptors (21). To ensure that our transgenic mice were typical of wild-type mice with the same background (C57BL/6j), experiments reported in Fig. 1 were repeated in both genotypes for comparison. There was no effect of genotype on rheobase, spike height, input resistance, or spiking pattern, nor was there any significant interaction between genotype and effects of TTX except for spike height at DIV4-7, where TTX had a marginally larger effect in wild-type mice (Two-way ANOVA, $F_{1,54}$=4.968, p=0.03, see source data file); therefore, we pooled the data for Fig.1. Having verified that our foundational observations held across different genotypes, we used transgenic mice for all subsequent experiments in order to identify eYFP-expressing nociceptors for patching, collection, or imaging.

Dorsal root ganglia neuron cultures

All key reagents are listed in **Supplementary Table 2**. Methods for primary DRG culture have been described previously (93). Briefly, adult mice (> 7 week-old) were anaesthetised with isoflurane and perfused intracardiacally with cold HBBS (without Ca and Mg, LifeTech 14170112) supplemented with (in mM) 15 HEPES, 28 Glucose, 111 sucrose, and pH adjusted with NaOH to 7.3-7.4; osmolarity 319-321. Lumbar dorsal root ganglia (DRGs) were extracted (L2-5, except for CFA-inflamed mice, in which we only took L4), digested with papain (Worthington Biochemical Corp.) and collagenase (Worthington Biochemical Corp.)/dispase II (Sigma), and mechanically dissociated by trituration before being plated onto poly-D lysine-coated coverslips and incubated in Neurobasal™ media (Gibco 21103-049) supplemented with 1 % fetal bovine serum (FBS), B-27™ supplement (Thermo Fisher 17504-044) and 0.5mM L-Glutamine (Gibco 25030-081) for an initial period of 2 hours. After this, media was changed to maintenance media (same as plating media but without FBS) and cells were maintained in a 5% CO_2 incubator at 37°C. Media was changed every 3-4 days thereafter. Neurons were recorded at two time points after plating: 2-8 hours (referred to as DIV0) or 4-7 days (referred to as DIV4-7). Neurons were tested at intermediate time points (DIV1-3) in the exploratory phase of our study but cellular heterogeneity prevented a clear picture of their TTX-sensitivity, presumably because different neurons shift from $Na_V1.8$ to $Na_V1.7$ at different rates. By DIV4, TTX sensitivity had stabilized, and so recordings from DIV4-7 were pooled for comparison with recordings on DIV0. When

tests were conducted on a specific day within the DIV4-7 range, the specific DIV is reported but should be considered representative of the DIV4-7 range. Additional experiments are required to determine the exact time course of the Na_V switch and its mechanistic basis; to mitigate effects of cellular heterogeneity, this would ideally involve techniques that allow longitudinal measurements in the same cell.

Electrophysiology

Coverslips with cultured neurons were transferred from the incubator to a recording chamber perfused with artificial cerebrospinal fluid containing (in mM): 126 NaCl, 2.5 KCl, 2.0 $CaCl_2$, 1.25 NaH_2PO_4, 26 $NaHCO_3$, 2 $MgCl_2$, and 10 glucose, bubbled with carbogen (5% CO_2:95% O_2) at room temperature. Neurons were visualized with gradient contrast optics on a Zeiss AxioExaminer microscope using a 40x, 0.75 NA water immersion objective (N-Achroplan, Zeiss) and IR-1000 Infrared CCD camera (Dage-MTI). YFP expression was visualized by epifluorescence (X-Cite, Excelitas) using a Zeiss filter set (46HE). A long-pass filter (OG590) was positioned in the transmitted light path to avoid activating ChR2 while patching. No optogenetic testing was performed as part of this study. Cells expressing YFP and with a soma diameter <25 µm were targeted for whole cell recording using pipettes (~5 MΩ resistance) pulled from borosilicate glass (WPI).

For current clamp recordings, pipettes were filled with intracellular solution containing (in Mm): 140 K-gluconate, 2 $MgCl_2$, 10 HEPES, 0.2 EGTA, 3.8 Na-ATP and 0.4 Na-GTP with pH adjusted to 7.3 with KOH; osmolarity was ~300 mOsm. A liquid junction potential correction of 15 mV was applied to all reported voltages. Series resistance was compensated to >70%. Signals were amplified with an Axopatch 200B amplifier (Molecular Devices, Sunnyvale, USA), low-pass filtered at 2 kHz, digitized with a Power1401 A/D device (Cambridge Electric Design, Cambridge, UK), and recorded at 10 kHz using CED software Signal version 6. After the natural resting membrane potential was noted, neurons were adjusted to -70 mV using continuous current injection in current clamp mode. Action potentials (spikes) were evoked using a series of 1-second long depolarizing current injections. Rheobase was defined as the minimal current required to evoke a spike. Neurons were tested with current injections from 1x rheobase to 4x rheobase using increments of 0.5x rheobase. Repetitive spiking neurons were defined as those producing ≥3 spikes in response to any stimulus intensity; transient spiking neurons consistently produced ≤2 spikes. Spike

threshold was defined as voltage where dV/dt first exceeds 5 mV/ms (94). Spike height was measured from threshold to peak of the action potential. Only neurons with a resting membrane potential below -45 mV, spikes overshooting 0 mV and recordings with <20% change in series resistance were tested and analyzed. For dynamic clamp experiments, the pipette shank was painted with Sylgard (Dow) to reduce pipette capacitance. Virtual $Na_V1.7$ and $Na_V1.8$ conductances were introduced into the cells using CED software Signal v6. Currents were defined using the Hodgkin-Huxley equation, using the same parameter values as in our computational model (see below).

For voltage-clamp recordings, the bath solution was adjusted to reduce sodium currents to ensure proper clamping (85). Bath solution contained (in mM): 65 NaCl, 50 choline chloride, 5 KCl, 5 HEPES, 5 $MgCl_2$, 10 glucose, and 0.1 $CaCl_2$, plus 0.1 $CdCl_2$ to block calcium currents, and 20 TEA and 5 4-AP to block potassium currents; pH was adjusted to 7.4 with NaOH. Pipettes were filled with intracellular solution containing (in Mm): 140 CsCl, 10 HEPES, 2 $MgCl_2$, 1 EGTA, 3.8 Na-ATP, 0.4 Na-GTP; pH was adjusted to 7.3 with CsOH. The resulting pipette resistance was ~3 MΩ. A liquid junction potential correction of 4.8 mV was applied to all command voltages. Sodium currents were recorded during 20 ms-long steps from -85 mV to voltages between -45 and +15 mV. Series resistance was compensated to >80%. Signals were amplified, low-pass filtered at 5 kHz, and digitized as described for current clamp recordings.

For all in vitro pharmacology, drugs were bath applied at a concentration chosen to selectively block the Na_V subtype of interest based on published EC50 values (see Supplementary Table 3)

Quantitative reverse transcription PCR (RT-qPCR)

Cultured DRG neurons <25 μm and expressing eYFP were identified as described above for patching. Coverslips were perfused with aCSF made with DEPC-treated ddH_2O, and identified neurons were collected using a glass pipette filled with intracellular solution also made from DEPC-treated ddH_2O (composition otherwise the same as described above for electrophysiology). Approximately 50 neurons were collected at DIV0 and at DIV4-7. Total mRNA was extracted with a PureLink RNA mini kit after digestion of genomic DNA with DNase I (Thermo Fisher Scientific) and the cDNA was synthesized with a SuperScript II first-strand

synthesis kit (Thermo Fisher Scientific) according to instructions. RT-qPCR was performed with the cDNA primers of target genes (**Supplementary Table 3**), and the PowerUp SYBR® Green master mix (Thermo Fisher Scientific) in the QuantStudio-3 real-time PCR system. The primers were designed with IDT and spanned at least one exon longer than 1000 bp in order to exclude contamination from genomic DNA. Non-RT mRNA was also used as a negative control to exclude contamination from genomic DNA. All target genes were performed in triplicate for each sample and the experiments were repeated at least 3 times. $Na_V1.7$ and $Na_V1.8$ transcript levels were analyzed using the 2-ΔΔCT method and compared with the housekeeping gene HPRT.

Immunocytochemistry

Cultured DRG neurons were treated with 4% paraformaldehyde for 10 minutes, rinsed 3x with cold PBS, and permeabilized with 0.1% Triton X-100 in PBS. After another 3x rinse with PBS, neurons were treated with 10% normal goat serum for 30 min followed with rabbit primary $Na_V1.7$ antibody (1:200, ASC-008, Alomone) or $Na_V1.8$ antibody (1:200, ASC-028, Alomone) in PBS with 0.1% Tritween-20 and 1% BSA for 1 h. For some of the coverslips, primary antibodies were replaced with control peptides (ASC008AG1040 for $Na_V1.7$ and ASC016AG0640 for $Na_V1.8$) provided by Alomone as negative controls. Following 3x rinse in PBS, neurons were incubated in the dark with goat anti-rabbit secondary antibody Alexa Fluor-647 (1:500, Abcam) in PBS containing 1% BSA for 1 h, followed by DAPI staining for 10 min. All incubations were done at room temperature. Finally, coverslips were mounted on slides with mounting media (Abcam, ab128982), imaged with a spinning disk confocal microscope (Quorum Technologies) using the same acquisition setting across all imaging sessions, and analyzed with Volocity software (v6.5.1). Protein levels are measured using fluorescence intensity and expressed relative to each other (e.g. ratios in Fig 6C) or relative to fluorescence intensity for YFP in the same cells. Each condition was tested in a minimum of 3 animals.

Behavioral testing

Behavioral tests were performed on adult mice (male and female, 8-12 weeks). Mice were acclimated to the testing environment for at least 1 h the day prior to start of experiments. Behavioral testing (von Frey

test and Hargreaves test) was then performed for 2-3 consecutive days for baseline and for another 3 days after CFA injection. Behavioral tests were performed at the same time in the morning, at room temperature (21°C) following a one-hour acclimation period. Animals were randomly assigned to experimental groups and the experimenter was blind to the drug condition.

CFA injection. CFA (Sigma, F5881) was thoroughly dissolved in saline (1:1) by vortexing the mixture. The resulting CFA solution (20 µl) was injected subdermally into the left hind paw under light isoflurane anaesthesia. The injection was performed shortly after the last baseline test, on Day 0.

PF-71 administration. Injectable PF-71 solution was prepared by first dissolving PF-71 in DMSO to make a 5% stock solution; dissolution was achieved by heating to 37°C and vortexing. On the day of injection, stock solution was dissolved in sunflower oil (5% v/v) by sonicating for 5 min. Freshly prepared final PF-71 solution was injected intraperitoneally (1 g/kg body weight). Behavioral testing was performed 2 hours after injection of PF-71 or vehicle.

Von Frey testing. Mechanical hyperalgesia was assessed with von Frey filaments (North Coast) using the SUDO method (95) . The average of 3 trials in each animal was used for analysis.

Hargreaves testing. Thermal hyperalgesia was assessed with the Hargreaves apparatus (Ugo Basile, Italy). Radiant heat was applied to the plantar surface of the left hind paw. Interval between stimulus onset and paw withdrawal was defined as paw withdrawal latency (PWL). A 20 s cut-off prevented damage to the skin if the animal failed to withdraw. The average of 3 trials in each animal was used for analysis.

Statistical analysis

Results are expressed as mean ± SEM when data are normally distributed or otherwise as median and quartiles. Normality was tested using the Kolmogorov-Smirnov test. Analysis was performed with GraphPad Prism (v9) and SigmaPlot (v11). Normally distributed data were compared using t-tests or two-way ANOVAs followed by a Student Newman-Keuls post hoc test. Non-normally distributed data were compared using Mann-Whitney and Wilcoxon signed rank tests. Fisher exact and McNemar test were used for categorical

data. Exact significance values and test results are reported throughout figure legends.

Computer model

Two separate, single compartmental models were built for DIV 0 and DIV4-7. They have the same, seven conductances: $g_{\mathrm{Nav1.3}}$, $g_{\mathrm{Nav1.7}}$, $g_{\mathrm{Nav1.8}}$, g_{Kdr}, g_{M}, g_{AHP} and g_{Leak}. Channel equations and their gating parameters are provided in **Supplementary Table 4**. Conductance densities at baseline (**Supplementary Table 5**) were tuned to qualitatively reproduce the changes in Na_V channel expressions at DIV 0 and 4-7 indicated by the experiments; changes to other channels were minimized between the two models. The effects of ICA, PF-71 and PF-24 were simulated by adjusting $\bar{g}_{\mathrm{Nav1.3}}$, $\bar{g}_{\mathrm{Nav1.7}}$ and $\bar{g}_{\mathrm{Nav1.8}}$, respectively, as reported in the figures. To re-introduce voltage noise that is otherwise missing from simulations, we included an Ornstein-Uhlenbeck process with μ_{noise} = 0 $\mu\mathrm{A/cm^2}$, σ_{noise} = 0.05 $\mu\mathrm{A/cm^2}$, and τ = 5 ms. All computer code is available at ModelDB (http://modeldb.yale.edu/267560; password: excitability). All simulations were conducted in MATLAB using the forward Euler integration method and a time step of 0.05–0.1 ms.

CONTRIBUTIONS: YX, SR, SAP designed the research; YX, JY collected data, YX, JY, SR, SAP analyzed data; YX, SR, SAP wrote the manuscript.

ACKNOWLEDGMENTS: This work was supported by a Restracomp fellowship to JY and by a Canadian Institutes of Health Research Foundation Grant (FDN167276) to SAP. We thank Rohini Kuner for providing Na_v1.8-Cre mice, Jason Jeong and Russell Smith for expert technical assistance with animal care and cell cultures, and Yongqian Wang for advice on qPCR data acquisition.

REFERENCES

1. Cohen SP, Vase L, & Hooten WM (2021) Chronic pain: an update on burden, best practices, and new advances. *Lancet* 397(10289):2082-2097.
2. Finnerup NB*, et al.* (2015) Pharmacotherapy for neuropathic pain in adults: a systematic review and meta-analysis. *Lancet Neurol* 14(2):162-173.
3. Rosenberger DC, Blechschmidt V, Timmerman H, Wolff A, & Treede RD (2020) Challenges of neuropathic pain: focus on diabetic neuropathy. *J Neural Trans* 127(4):589-624.
4. Hay M, Thomas DW, Craighead JL, Economides C, & Rosenthal J (2014) Clinical development success rates for investigational drugs. *Nat Biotechnol* 32(1):40-51.
5. Woolf CJ (2010) Overcoming obstacles to developing new analgesics. *Nat Med* 16(11):1241-1247.
6. Mogil JS (2009) Animal models of pain: progress and challenges. *Nat Rev Neurosci* 10(4):283-294.
7. Taneja A, Di Iorio VL, Danhof M, & Della Pasqua O (2012) Translation of drug effects from experimental models of neuropathic pain and analgesia to humans. *Drug Discov Today* 17(15-16):837-849.
8. Mao J (2012) Current challenges in translational pain research. *Trends Pharmacol Sci* 33(11):568-573.
9. Edelman GM & Gally JA (2001) Degeneracy and complexity in biological systems. *Proc Natl Acad Sci U S A* 98(24):13763-13768.
10. Ratté S & Prescott SA (2016) Afferent hyperexcitability in neuropathic pain and the inconvenient truth about its degeneracy. *Curr Opin Neurobiol* 36:31-37.
11. Gold MS & Gebhart GF (2010) Nociceptor sensitization in pain pathogenesis. *Nat Med* 16(11):1248-1257.
12. Haroutounian S*, et al.* (2014) Primary afferent input critical for maintaining spontaneous pain in peripheral neuropathy. *Pain* 155(7):1272-1279.
13. Yatziv SL & Devor M (2019) Suppression of neuropathic pain by selective silencing of dorsal root ganglion ectopia using nonblocking concentrations of lidocaine. *Pain* 160(9):2105-2114.
14. Alles SRA & Smith PA (2021) Peripheral voltage-gated cation channels in neuropathic pain and their potential as therapeutic targets. *Front Pain Res* 2:750583.
15. Bean BP (2007) The action potential in mammalian central neurons. *Nat Rev Neurosci.* 8(6):451-465.
16. Waxman SG & Zamponi GW (2014) Regulating excitability of peripheral afferents: emerging ion channel targets. *Nat Neurosci* 17(2):153-163.
17. Cox JJ*, et al.* (2006) An SCN9A channelopathy causes congenital inability to experience pain. *Nature* 444(7121):894-898.
18. Fertleman CR*, et al.* (2006) SCN9A mutations in paroxysmal extreme pain disorder: allelic variants underlie distinct channel defects and phenotypes. *Neuron* 52(5):767-774.
19. Yang Y*, et al.* (2004) Mutations in SCN9A, encoding a sodium channel alpha subunit, in patients with primary erythermalgia. *J Med Genet* 41(3):171-174.
20. Dib-Hajj SD, Yang Y, Black JA, & Waxman SG (2013) The $Na_V1.7$ sodium channel: from molecule to man. *Nat Rev Neurosci* 14(1):49-62.
21. Nassar MA*, et al.* (2004) Nociceptor-specific gene deletion reveals a major role for $Na_V1.7$ (PN1) in acute and inflammatory pain. *Proc Natl Acad Sci U S A* 101(34):12706-12711.

22. Nassar MA, Levato A, Stirling LC, & Wood JN (2005) Neuropathic pain develops normally in mice lacking both $Na_V1.7$ and $Na_V1.8$. *Mol Pain* 1(24):24.

23. Minett MS*, et al.* (2014) Pain without nociceptors? $Na_V1.7$-independent pain mechanisms. *Cell Rep* 6(2):301-312.

24. Grubinska B*, et al.* (2019) Rat $Na_V1.7$ loss-of-function genetic model: Deficient nociceptive and neuropathic pain behavior with retained olfactory function and intra-epidermal nerve fibers. *Mol Pain* 15:1744806919881846.

25. Minett MS*, et al.* (2012) Distinct $Na_V1.7$-dependent pain sensations require different sets of sensory and sympathetic neurons. *Nat Commun* 3:791.

26. Shields SD*, et al.* (2018) Insensitivity to pain upon adult-onset deletion of $Na_V1.7$ or its blockade with selective inhibitors. *J Neurosci* 38(47):10180-10201.

27. MacDonald DI*, et al.* (2021) A central mechanism of analgesia in mice and humans lacking the sodium channel $Na_V1.7$. *Neuron* 109(9):1497-1512.e1496.

28. Minett MS*, et al.* (2015) Endogenous opioids contribute to insensitivity to pain in humans and mice lacking sodium channel $Na_V1.7$. *Nat Commun* 6:8967.

29. Dehen H, Willer JC, Prier S, Boureau F, & Cambier J (1978) Congenital insensitivity to pain and the "morphine-like" analgesic system. *Pain* 5(4):351-358.

30. Emery EC, Luiz AP, & Wood JN (2016) $Na_V1.7$ and other voltage-gated sodium channels as drug targets for pain relief. *Expert Opin Ther Targets* 20(8):975-983.

31. Vetter I*, et al.* (2017) $Na_V1.7$ as a pain target - From gene to pharmacology. *Pharmacol Ther* 172:73-100.

32. Yang Y, Mis MA, Estacion M, Dib-Hajj SD, & Waxman SG (2018) $Na_V1.7$ as a pharmacogenomic Ttrget for pain: moving toward precision medicine. *Trends Pharmacol Sci* 39(3):258-275.

33. Kushnarev M, Pirvulescu IP, Candido KD, & Knezevic NN (2020) Neuropathic pain: preclinical and early clinical progress with voltage-gated sodium channel blockers. *Expert opin Investig Drugs* 29(3):259-271.

34. Alsaloum M, Higerd GP, Effraim PR, & Waxman SG (2020) Status of peripheral sodium channel blockers for non-addictive pain treatment. *Nat Rev Neurol* 16(12):689-705.

35. Eagles DA, Chow CY, & King GF (2022) Fifteen years of Na_V 1.7 channels as an analgesic target: Why has excellent in vitro pharmacology not translated into in vivo analgesic efficacy? *Br J Pharmacol* 179(14):3592-3611.

36. Kitano Y & Shinozuka T (2022) Inhibition of $Na_V1.7$: the possibility of ideal analgesics. *RSC Med Chem* 13(8):895-920.

37. Mulcahy JV*, et al.* (2019) Challenges and opportunities for therapeutics targeting the voltage-gated sodium channel isoform $Na_V1.7$. *J Med Chem* 62(19):8695-8710.

38. Bankar G*, et al.* (2018) Selective NaV1.7 Antagonists with long residence time show improved efficacy against inflammatory and neuropathic pain. *Cell Rep* 24(12):3133-3145.

39. Kingwell K (2019) $Na_V1.7$ withholds its pain potential. *Nat Rev Drug Discov* 18:321-323.

40. Alexandrou AJ*, et al.* (2016) Subtype-selective small molecule inhibitors reveal a fundamental role for $Na_V1.7$ in nociceptor electrogenesis, axonal conduction and presynaptic release. *PLoS One* 11(4):e0152405.

41. McDermott LA*, et al.* (2019) Defining the functional role of $Na_V1.7$ in human nociception. *Neuron* 101(5):905-919.e908.

42. Rothenberg ME*, et al.* (2019) Safety, tolerability, and pharmacokinetics of GDC-0276, a novel $Na_V1.7$ inhibitor, in a first-in-human, single- and multiple-dose study in healthy volunteers. *Clin Drug Investig* 39(9):873-887.

43. Flake NM, Lancaster E, Weinreich D, & Gold MS (2004) Absence of an association between axotomy-induced changes in sodium currents and excitability in DRG neurons from the adult rat. *Pain* 109(3):471-480.

44. Zhang JM, Donnelly DF, Song XJ, & LaMotte RH (1997) Axotomy increases the excitability of dorsal root ganglion cells with unmyelinated axons. *J Neurophysiol* 78(5):2790-2794.

45. Amir R, Michaelis M, & Devor M (1999) Membrane potential oscillations in dorsal root ganglion neurons: role in normal electrogenesis and neuropathic pain. *J Neurosci* 19(19):8589-8596.

46. Caffrey JM, Eng DL, Black JA, Waxman SG, & Kocsis JD (1992) Three types of sodium channels in adult rat dorsal root ganglion neurons. *Brain Res* 592(1-2):283-297.

47. Renganathan M, Cummins TR, & Waxman SG (2001) Contribution of $Na_V1.8$ sodium channels to action potential electrogenesis in DRG neurons. *J Neurophysiol* 86(2):629-640.

48. Rush AM, Cummins TR, & Waxman SG (2007) Multiple sodium channels and their roles in electrogenesis within dorsal root ganglion neurons. *J Physiol* 579(Pt 1):1-14.

49. Zhang JM, Song XJ, & LaMotte RH (1999) Enhanced excitability of sensory neurons in rats with cutaneous hyperalgesia produced by chronic compression of the dorsal root ganglion. *J Neurophysiol* 82(6):3359-3366.

50. Payne CE*, et al.* (2015) A novel selective and orally bioavailable $Na_V1.8$ channel blocker, PF-01247324, attenuates nociception and sensory neuron excitability. *Br J Pharmacol* 172(10):2654-2670.

51. Vijayaragavan K, O'Leary ME, & Chahine M (2001) Gating properties of $Na_V1.7$ and $Na_V1.8$ peripheral nerve sodium channels. *J Neurosci* 21(20):7909-7918.

52. Theile JW, Fuller MD, & Chapman ML (2016) The selective $Na_V1.7$ inhibitor, PF-05089771, interacts equivalently with fast and slow inactivated $Na_V1.7$ channels. *Molec Pharmacol* 90(5):540-548.

53. McCormack K*, et al.* (2013) Voltage sensor interaction site for selective small molecule inhibitors of voltage-gated sodium channels. *Proc Natl Acad Sci U S A* 110(29):E2724-2732.

54. Strege PR*, et al.* (2017) Sodium channel $Na_V1.3$ is important for enterochromaffin cell excitability and serotonin release. *Sci Rep* 7(1):15650.

55. Osteen JD*, et al.* (2016) Selective spider toxins reveal a role for the $Na_V1.1$ channel in mechanical pain. *Nature* 534(7608):494-499.

56. Bennett DL, Clark AJ, Huang J, Waxman SG, & Dib-Hajj SD (2019) The role of voltage-gated sodium channels in pain signaling. *Physiol Rev* 99(2):1079-1151.

57. Prescott SA, De Koninck Y, & Sejnowski TJ (2008) Biophysical basis for three distinct dynamical mechanisms of action potential initiation. *PLoS Comput.Biol.* 4(10):e1000198.

58. Berta T*, et al.* (2008) Transcriptional and functional profiles of voltage-gated Na^+ channels in injured and non-injured DRG neurons in the SNI model of neuropathic pain. *Mol Cell Neurosci* 37(2):196-208.

59. Dustrude ET, Wilson SM, Ju W, Xiao Y, & Khanna R (2013) CRMP2 protein SUMOylation modulates $Na_V1.7$ channel trafficking. *J Biol Chem* 288(34):24316-24331.

60. Yamane M*, et al.* (2017) A functional coupling between CRMP1 and $Na_V1.7$ for retrograde propagation of Semaphorin3A signaling. *J Cell Sci* 130(8):1393-1403.

61. Gould HJ, 3rd, England JD, Liu ZP, & Levinson SR (1998) Rapid sodium channel augmentation in response to inflammation induced by complete Freund's adjuvant. *Brain Res* 802(1-2):69-74.

62. Black JA, Liu S, Tanaka M, Cummins TR, & Waxman SG (2004) Changes in the expression of tetrodotoxin-sensitive sodium channels within dorsal root ganglia neurons in inflammatory pain. *Pain* 108(3):237-247.

63. Liang L, Fan L, Tao B, Yaster M, & Tao YX (2013) Protein kinase B/Akt is required for complete Freund's adjuvant-induced upregulation of Nav1.7 and Nav1.8 in primary sensory neurons. *J Pain* 14(6):638-647.

64. Akin EJ*, et al.* (2019) Building sensory axons: Delivery and distribution of $Na_V1.7$ channels and effects of inflammatory mediators. *Sci Adv* 5(10):eaax4755.

65. Moreno AM*, et al.* (2021) Long-lasting analgesia via targeted in situ repression of $Na_V1.7$ in mice. *Sci Transl Med* 13(584).

66. Baron R & Dickenson AH (2014) Neuropathic pain: precise sensory profiling improves treatment and calls for back-translation. *Pain* 155(11):2215-2217.

67. Marder E & Goaillard JM (2006) Variability, compensation and homeostasis in neuron and network function. *Nat Rev Neurosci* 7(7):563-574.

68. O'Leary T, Williams AH, Franci A, & Marder E (2014) Cell types, network homeostasis, and pathological compensation from a biologically plausible ion channel expression model. *Neuron* 82(4):809-821.

69. Drion G, O'Leary T, & Marder E (2015) Ion channel degeneracy enables robust and tunable neuronal firing rates. *Proc Natl Acad Sci U S A* 112(38):E5361-5370.

70. Mishra P & Narayanan R (2022) Conjunctive changes in multiple ion channels mediate activity-dependent intrinsic plasticity in hippocampal granule cells. *iScience* 25(3):103922.

71. Yang J, Shakil H, Ratté S, & Prescott SA (2022) Minimal requirements for a neuron to coregulate many properties and the implications for ion channel correlations and robustness. *Elife* 11:e72875.

72. Drion G, Massotte L, Sepulchre R, & Seutin V (2011) How modeling can reconcile apparently discrepant experimental results: the case of pacemaking in dopaminergic neurons. *PLoS Comput Biol* 7(5):e1002050.

73. Puopolo M, Raviola E, & Bean BP (2007) Roles of subthreshold calcium current and sodium current in spontaneous firing of mouse midbrain dopamine neurons. *J Neurosci* 27(3):645-656.

74. Swensen AM & Bean BP (2005) Robustness of burst firing in dissociated purkinje neurons with acute or long-term reductions in sodium conductance. *J Neurosci* 25(14):3509-3520.

75. Knox AT, Glauser T, Tenney J, Lytton WW, & Holland K (2018) Modeling pathogenesis and treatment response in childhood absence epilepsy. *Epilepsia* 59(1):135-145.

76. Prinz AA, Bucher D, & Marder E (2004) Similar network activity from disparate circuit parameters. *Nat Neurosci* 7(12):1345-1352.

77. Grashow R, Brookings T, & Marder E (2010) Compensation for variable intrinsic neuronal excitability by circuit-synaptic interactions. *J Neurosci* 30(27):9145-9156.

78. Medlock L*, et al.* (2022) Multiscale computer model of the spinal dorsal horn reveals changes in network processing associated with chronic pain. *J Neurosci* 42(15):3133-3149.

79. Prescott SA, Sejnowski TJ, & De Koninck Y (2006) Reduction of anion reversal potential subverts the inhibitory control of firing rate in spinal lamina I neurons: towards a biophysical basis for neuropathic pain. *Mol Pain* 2:32.

80. Lee KY & Prescott SA (2015) Chloride dysregulation and inhibitory receptor blockade yield equivalent disinhibition of spinal neurons yet are differentially reversed by carbonic anhydrase blockade. *Pain* 156(12):2431-2437.

81. Djouhri L*, et al.* (2003) Sensory and electrophysiological properties of guinea-pig sensory neurones expressing $Na_V1.7$ (PN1) Na^+ channel alpha subunit protein. *J Physiol* 546(Pt 2):565-576.

82. Campbell JN, Raja SN, Meyer RA, & Mackinnon SE (1988) Myelinated afferents signal the hyperalgesia associated with nerve injury. *Pain* 32(1):89-94.

83. Koltzenburg M, Lundberg LE, & Torebjork HE (1992) Dynamic and static components of mechanical hyperalgesia in human hairy skin. *Pain* 51(2):207-219.

84. Liu CN*, et al.* (2000) Tactile allodynia in the absence of C-fiber activation: altered firing properties of DRG neurons following spinal nerve injury. *Pain* 85(3):503-521.

85. Liu X, Eschenfelder S, Blenk KH, Jänig W, & Häbler H (2000) Spontaneous activity of axotomized afferent neurons after L5 spinal nerve injury in rats. *Pain* 84(2-3):309-318.

86. Abrahamsen B*, et al.* (2008) The cell and molecular basis of mechanical, cold, and inflammatory pain. *Science* 321(5889):702-705.

87. Goaillard JM & Marder E (2021) Ion channel degeneracy, variability, and covariation in neuron and circuit resilience. *Annu Rev Neurosci* 44:335-357.

88. Yang J & Prescott SA (2023) Homeostatic regulation of neuronal function: importance of degeneracy and pleiotropy. *Front Cell Neurosci* 17:1184563.

89. Schild JH & Kunze DL (1997) Experimental and modeling study of Na^+ current heterogeneity in rat nodose neurons and its impact on neuronal discharge. *J Neurophysiol* 78(6):3198-3209.

90. Blair NT & Bean BP (2002) Roles of tetrodotoxin (TTX)-sensitive Na^+ current, TTX-resistant Na^+ current, and Ca^{2+} current in the action potentials of nociceptive sensory neurons. *J Neurosci* 22(23):10277-10290.

91. Stober TM, Batulin D, Triesch J, Narayanan R, & Jedlicka P (2023) Degeneracy in epilepsy: Multiple routes to hyperexcitable brain circuits and their repair. *Commun Biol* 6(6):479.

92. Agarwal N, Offermanns S, & Kuner R (2004) Conditional gene deletion in primary nociceptive neurons of trigeminal ganglia and dorsal root ganglia. *Genesis* 38(3):122-129.

93. Malin SA, Davis BM, & Molliver DC (2007) Production of dissociated sensory neuron cultures and considerations for their use in studying neuronal function and plasticity. *Nat Protoc* 2(1):152-160.

94. Davidson S*, et al.* (2014) Human sensory neurons: Membrane properties and sensitization by inflammatory mediators. *Pain* 155(9):1861-1870.

95. Bonin RP, Bories C, & De Koninck Y (2014) A simplified up-down method (SUDO) for measuring mechanical nociception in rodents using von Frey filaments. *Mol Pain* 10:26.

96. Renganathan M, Dib-Hajj S, & Waxman SG (2002) $Na_V1.5$ underlies the 'third TTX-R sodium current' in rat small DRG neurons. *Brain Res Mol Brain Res* 106(1-2):70-82.

97. Jarvis MF*, et al.* (2007) A-803467, a potent and selective $Na_V1.8$ sodium channel blocker, attenuates neuropathic and inflammatory pain in the rat. *Proc Natl Acad Sci U S A* 104(20):8520-8525.

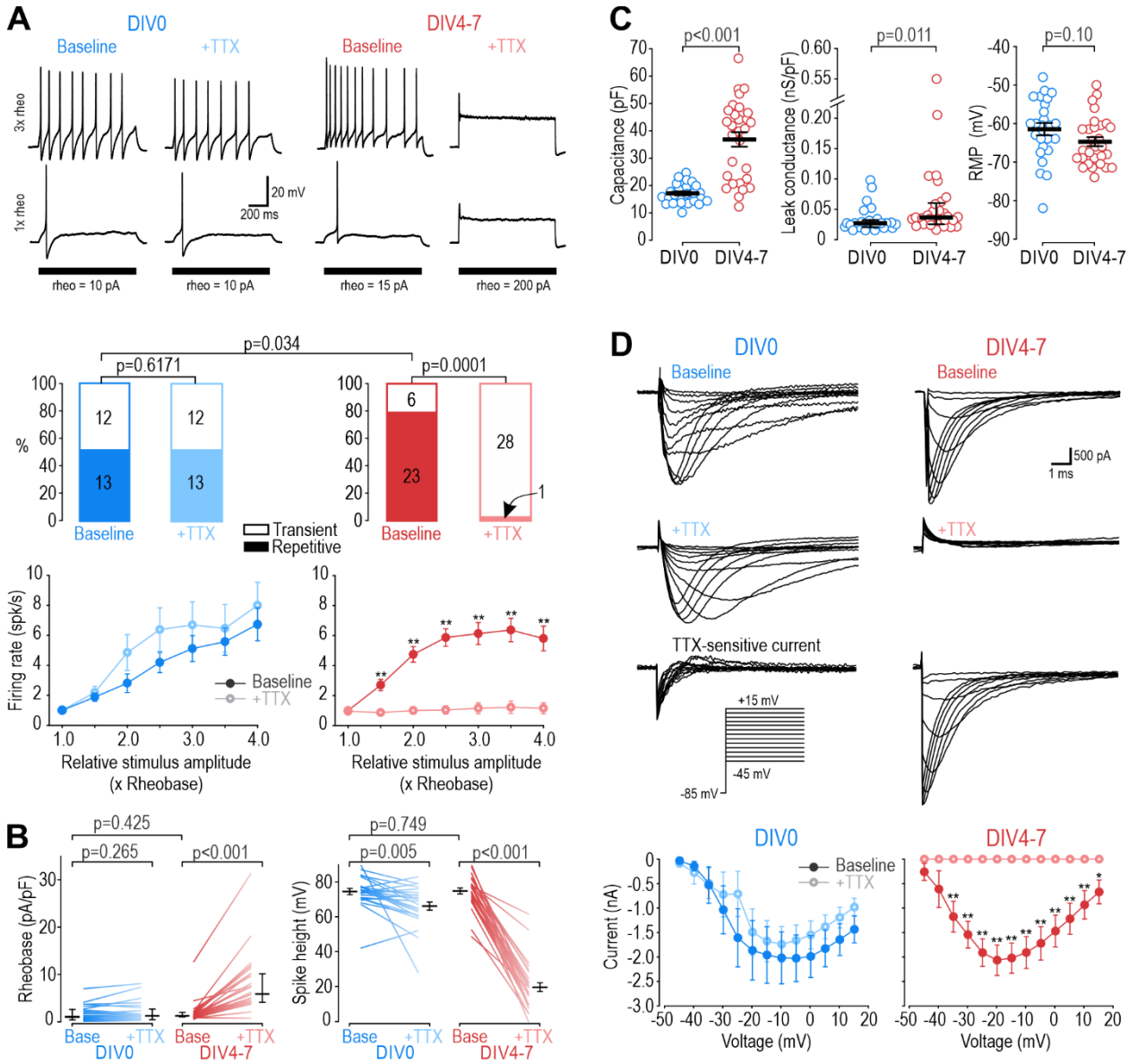

Figure 1. Different Na_V subtypes produce equivalent excitability at different days in vitro (DIV).

(A) Representative responses of small DRG neurons to current injection at rheobase and 3x rheobase when tested on DIV0 (blue) or DIV4-7 (red) before (dark) and after (pale) bath application of 100 nM TTX. At DIV0, TTX did not alter spiking pattern (χ^2=0.25, p=0.617, McNemar test) or significantly reduce firing rate ($F_{1,72}$=1.527, p=0.24, two-way repeated measure (RM) ANOVA; n=13). At DIV4-7, TTX significantly altered spiking pattern, converting all but one neuron to transient spiking (χ^2=20.05, p<0.0001), and it significantly reduced firing rate ($F_{1,132}$=43.157, p<0.001, n=23). Only neurons with repetitive spiking at baseline are included in the firing rate plot. **(B)** At DIV0, TTX did not affect rheobase (Z_{24}=1.129, p=0.265, Wilcoxon rank test) but did reduce spike height (T_{24}=3.092, p=0.005, paired t-test). At DIV4-7, TTX increased rheobase (Z_{28}=4.681, p<0.001, Wilcoxon rank test) and dramatically reduced spike height (T_{28}=20.333, p<0.001, paired t-test). Notably, neurons at DIV0 and DIV4-7 did not differ in their baseline rheobase (U=316, p=0.425,

Mann-Whitney test) or spike height (T_{52}=0.322, p=0.749, t-test). **(C)** Neurons at DIV0 and DIV4-7 differed in their total capacitance (T_{52}=6.728, p<0.001, t-test) and leak conductance density (U=216, p=0.011, Mann-Whitney test) but not in their resting membrane potential (T_{52}=1.668, p=0.101, t-test). **(D)** Sample voltage clamp recordings with command voltage stepped from -85 mV to +15 mV in 5 mV increments, before and after TTX. Sodium current was not significantly reduced by TTX at DIV0 ($F_{1,72}$=3.585, p=0.107, two-way RM ANOVA; n=7 neurons) but was completely abolished by TTX at DIV4-7 ($F_{1,108}$=33.526, p<0.001; n=10 neurons). *, p<0.05; **, p<0.01; Student- Newman-Keuls post-hoc tests in A and D. Traces labeled "TTX-sensitive current" represent the difference between current measured at baseline and after TTX, as determined by subtracting responses to the same voltage step under different pharmacological conditions.

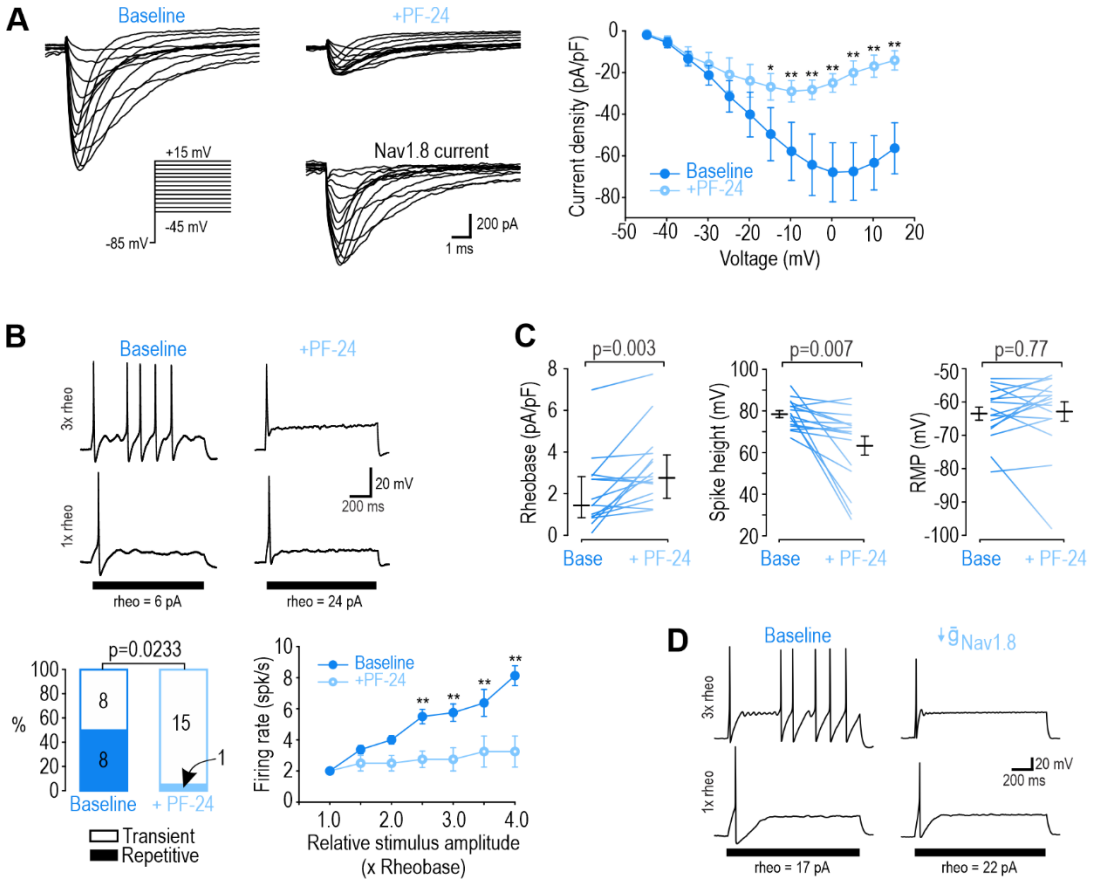

Figure 2. $Na_V1.8$ is necessary for repetitive spiking at DIV0.

(A) Sample voltage clamp recordings show that sodium current was almost completely abolished by the $Na_V1.8$ inhibitor PF-24 (1 µM). Peak current was significantly reduced by PF-24 ($F_{1,72}$=12.651, p<0.012, two-way RM ANOVA; n=7). Traces labeled "$Na_V1.8$ current" represent the difference between current measured at baseline and after PF-24, as determined by subtraction. Another $Na_V1.8$ inhibitor, A-803467, had a similar effect (see Fig. 2 – figure supplement 1). **(B)** PF-24 significantly altered spiking pattern (χ^2=5.14, p=0.0233, McNemar test) and reduced firing rate ($F_{1,42}$=11.946, p=0.011, two-way RM ANOVA; n=8). **(C)** PF-24 significantly increased rheobase (Z_{15}=2.783, p=0.003, Wilcoxon rank test) and reduced spike height (T_{15}=3.151, p=0.007, paired t-test) but did not affect resting membrane potential (T_{15}=0.304, p=0.765, paired t-test). PF-24 had limited effects at DIV4-7 (Fig 2 – figure supplement 2). **(D)** A computational model reproduced the effect of $Na_V1.8$ on spiking pattern (also see Supplementary Table 1). The PF-24 effect was simulated as a ~85% reduction in $Na_V1.8$ ($\bar{g}_{\mathrm{Nav1.8}}$= 4mS/cm2). *, p<0.05; **; p<0.01; Student-Newman-Keuls post-hoc tests in A and B.

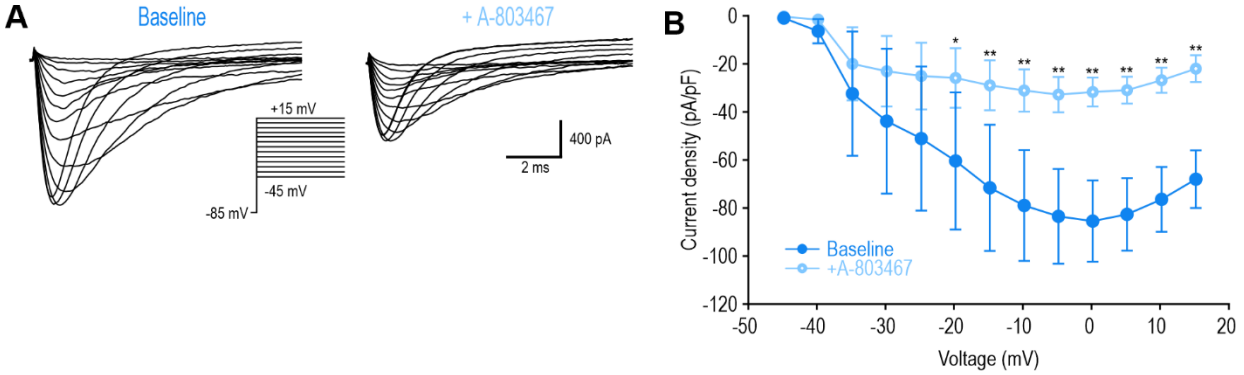

Figure 2 – figure supplement 1. Inhibiting $Na_V1.8$ at DIV0 with A-803467 had the same effect as PF-24.

(A) Sample voltage clamp recording at DIV0 before and after A-803467 (1 µM). **(B)** Peak current was significantly reduced by A-803467 ($F_{1,84}$=9.935, p=0.016, two-way RM ANOVA, n=8). *, p<0.05; **, p<0.01; Student-Newman-Keuls post-hoc test in B.

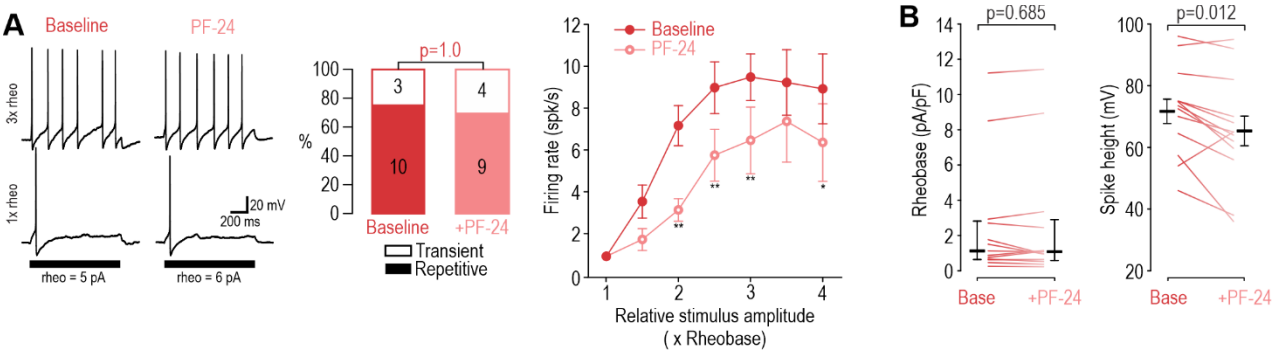

Figure 2 – figure supplement 2. Inhibiting $Na_V1.8$ with PF-24 at DIV4-7 had negligible effects.

(A) Inhibiting $Na_v1.8$ with PF-24 (1 µM) did not affect spiking pattern (χ^2 =0.00, p=1.00, McNemar test) and modestly reduced firing rate ($F_{1,54}$=9.745, p= 0.012, two-way RM ANOVA, n=10) in DIV4-7 neurons. **(B)** PF-24 did not affect rheobase (Z_{12}=0.420, p=0.685, Wilcoxon Rank test) but did reduce spike height (T12=2.939, p=0.012, paired-t-test). *, p<0.05; **, p<0.01; Student-Newman-Keuls post-hoc tests in A.

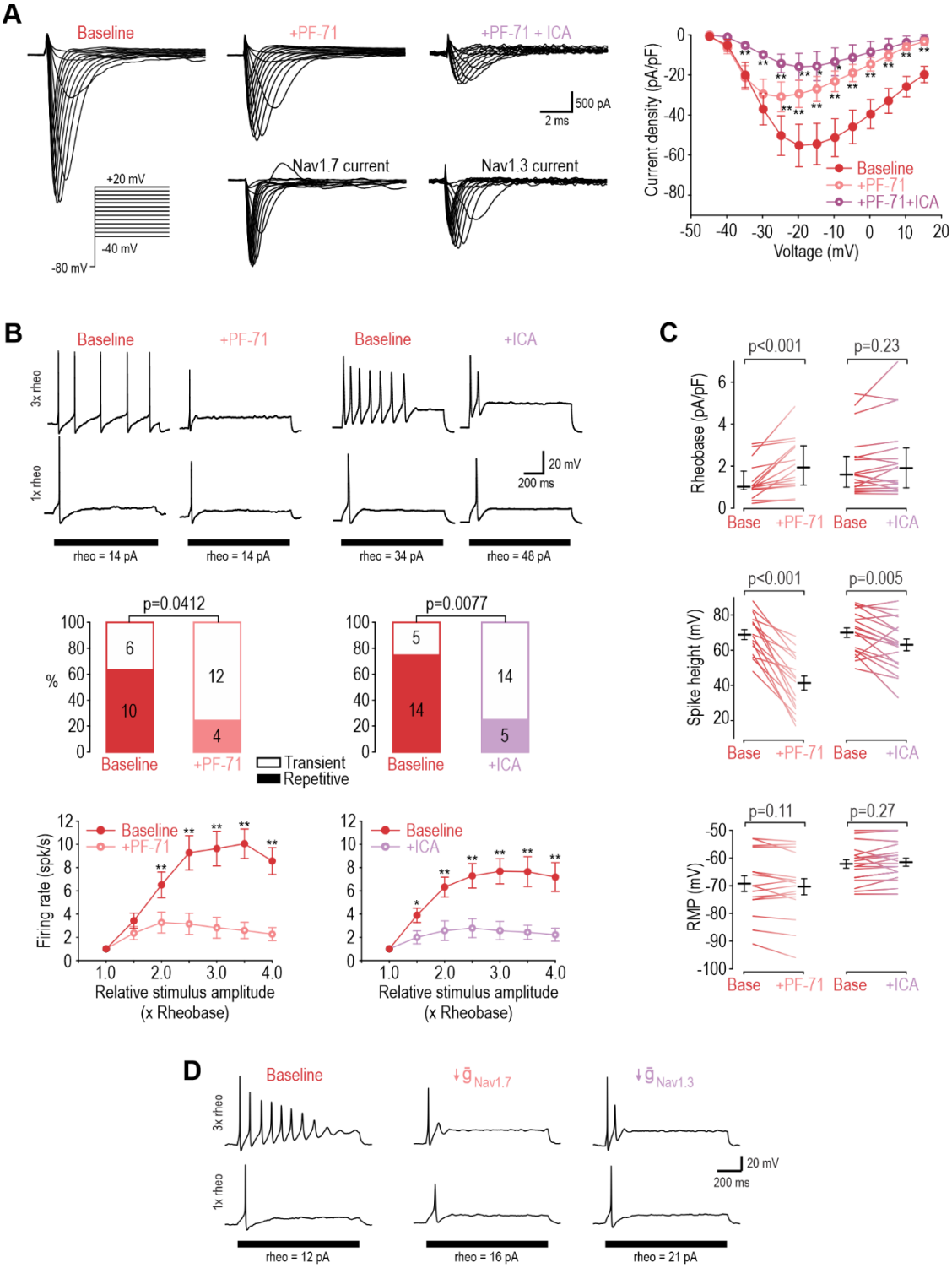

Figure 3. $Na_V1.3$ and $Na_V1.7$ are necessary for repetitive spiking at DIV4-7.

(A) Sample voltage clamp recordings show that sodium current was reduced by the $Na_V1.7$ inhibitor PF-71 (30 nM) and by the $Na_V1.1/1.3$ inhibitor ICA (1 µM). Peak current was significantly reduced by PF-71 and ICA ($F_{2,192}$=26.361, p<0.001, two-way RM ANOVA; n=9). Traces labeled "$Na_V1.7$ current" and "$Na_V1.3$ current" represent the difference between current measured at baseline and after PF-72 and ICA,

respectively, as determined by subtraction. **(B)** PF-71 and ICA both significantly altered spiking pattern (χ^2=4.17, p=0.041 and χ^2 =7.11, p=0.0077, respectively, McNemar tests) and significantly reduced firing rate ($F_{1,54}$=40.659, p<0.001, n=10 and $F_{1,78}$=35.156, p<0.001, n=14, respectively, two-way RM ANOVAs). **(C)** PF-71 significantly increased rheobase (Z_{18}=3.464, p<0.001, Wilcoxon rank test) and decreased spike height (T_{18}=7.946, p<0.001, paired t-test). ICA did not significantly alter rheobase (Z_{18}=1.248, p=0.225) but did reduce spike height (T_{18}=3.243, p=0.005). Neither drug affected resting membrane potential (T_{15}=1.681, p=0.113 for PF-71; T_{18}=-1.132, p=0.272 for ICA, paired t-test). PF-71 had negligible effects at DIV0 (Fig. 3 – figure supplement 1). **(D)** A computational model reproduced the combined effects of $Na_V1.3$ and $Na_V1.7$ on spiking pattern (also see Supplementary Table 1 and Fig. 3 – figure supplement 2). PF-71 effect was simulated as a 70% reduction in $Na_V1.7$ ($\bar{g}_{\mathrm{Nav1.7}}$= 10.5 mS/cm^2). ICA effect was simulated as a 90% reduction in $Na_V1.3$ ($\bar{g}_{\mathrm{Nav1.3}}$= 0.035 mS/cm^2). *, p<0.05; **, p<0.01; Student-Newman-Keuls post-hoc tests in A and B.

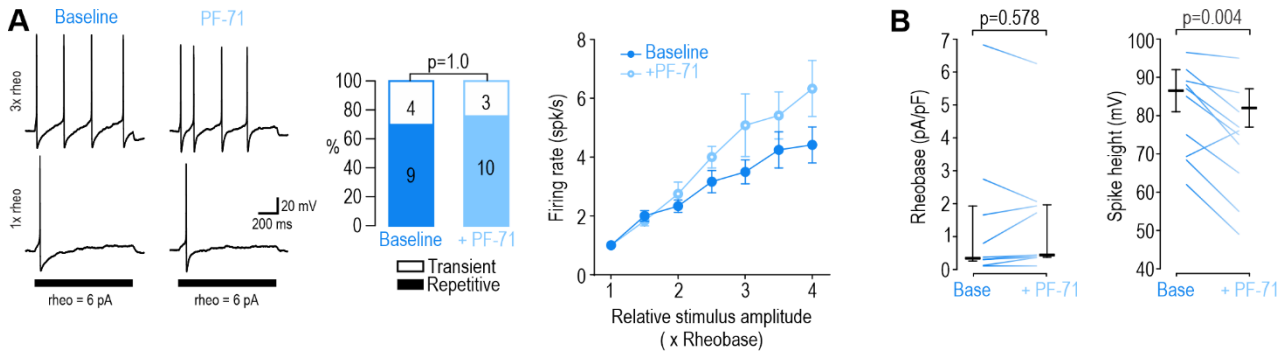

Figure 3 – figure supplement 1. Inhibiting $Na_V1.7$ at DIV0 had negligible effects.

(A) Inhibiting $Na_V1.7$ with PF-71 (30 nM) did not alter spiking pattern (χ^2=0.00, p=1.00, McNemar test) or reduce firing rate ($F_{1,30}$=5.805, p=0.061, two-way RM ANOVA, n=6) in DIV0 neurons; in fact, firing rate was slightly increased. **(D-E)** PF-71 did not affect rheobase (Z_9=0.677, p=0.578, Wilcoxon rank test) but did reduce spike height (T_9=3.759, p=0.004, paired-t-test).

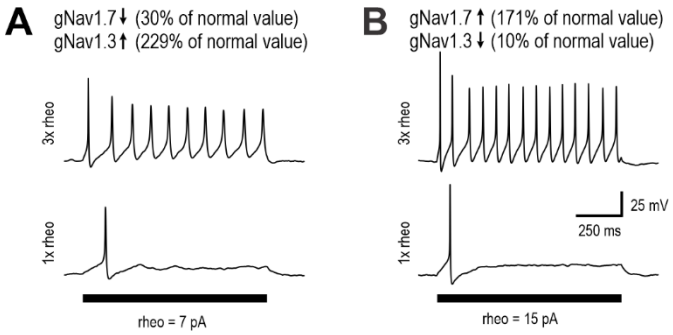

Figure 3 – figure supplement 2. $Na_V1.7$ and $Na_V1.3$ currents can compensate for each other.

(A) In the DIV4-7 model, reducing $\bar{g}_{\mathrm{Nav1.7}}$ to 30% of its normal value (35→10 mS/cm^2) can be compensated for by increasing $\bar{g}_{\mathrm{Nav1.3}}$ to 229% of its normal value (0.35→0.8 mS/cm^2) to maintain repetitive spiking. **(B)** Conversely, reducing $\bar{g}_{\mathrm{Nav1.3}}$ to 10% of its normal value (0.35→0.035 mS/cm^2) can be compensated for by increasing $\bar{g}_{\mathrm{Nav1.7}}$ to 171% of its normal value (35→60 mS/cm^2) and maintain repetitive spiking.

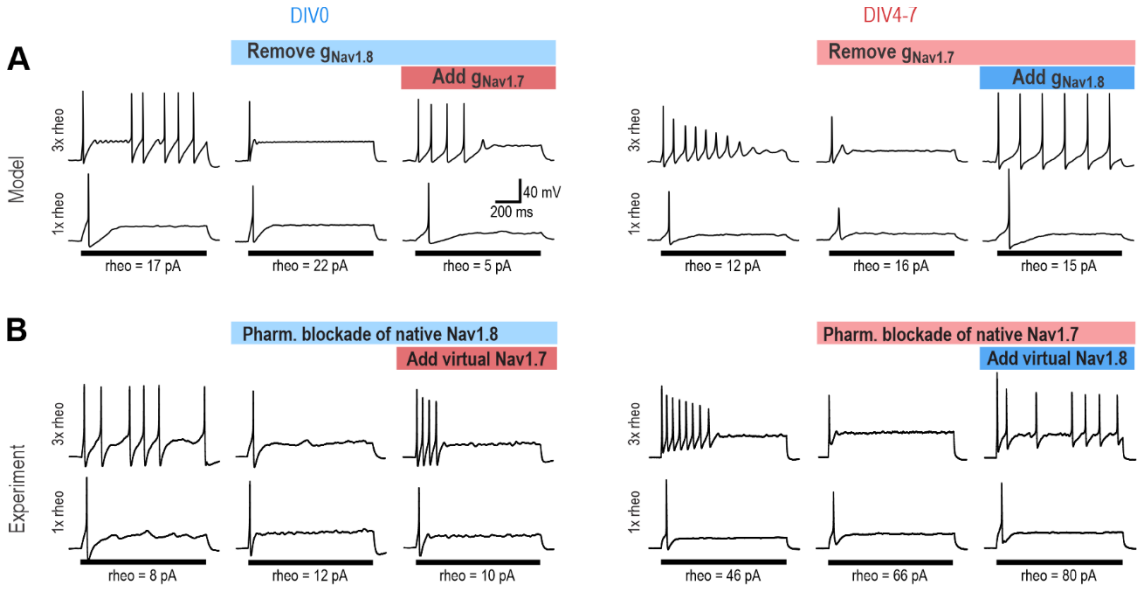

Figure 4. $Na_V1.7$ and $Na_V1.8$ are each sufficient to produce repetitive spiking in DIV0 and DIV4-7 neurons. (A) The computational model predicts that the $Na_V1.8$ conductance, which is "necessary" for repetitive spiking at DIV0 can, in principle, be replaced by $Na_V1.7$ (left), and vice versa at DIV4-7 (right). **(B)** Replacement experiments involved inhibiting native channels pharmacologically and then introducing virtual conductances using dynamic clamp. At DIV0 (left), inhibiting native $Na_V1.8$ (with PF-24) converted neurons to transient spiking, but introducing virtual $Na_V1.7$ reverted neurons to repetitive spiking (in 3 of 3 neurons tested). At DIV4-7, inhibiting native $Na_V1.7$ (with PF-71) converted the neuron to transient spiking, but introducing virtual $Na_V1.8$ reverted neurons to repetitive spiking (in 4 of 4 neurons tested). Repetitive spiking was likewise restored by replacing the blocked native channel with the corresponding virtual channel (**Fig. 4 – figure supplement 1**). Parameters for virtual channels were identical to simulations except for the maximal conductance density, which was titrated in each cell.

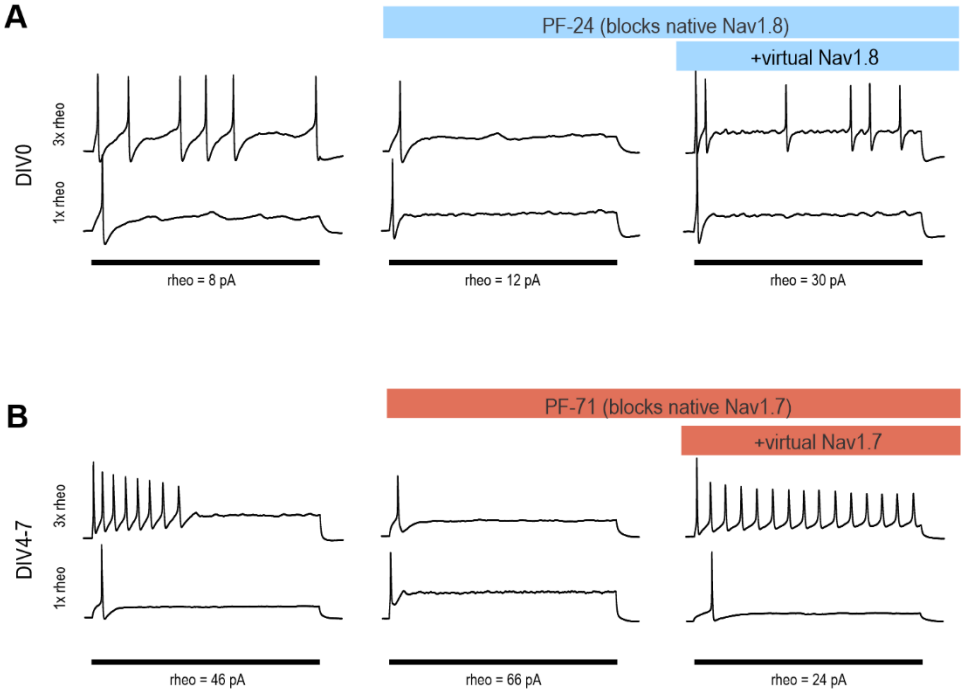

Figure 4 – figure supplement 1. Virtual conductances restored repetitive spiking after pharmacological inhibition of the corresponding native conductance had converted the neuron to transient spiking.

(A) Sample response at DIV0 showing that a virtual $Na_V1.8$ conductance applied with dynamic clamp restored repetitive spiking after inhibiting native $Na_V1.8$ channels with PF-24. This restoration was repeated in 3 of 3 neurons tested. **(B)** Sample recording at DIV4-7 showing that a virtual $Na_V1.7$ conductance restored repetitive spiking after inhibiting native $Na_V1.7$ channels with PF-71. This restoration was repeated in 4 of 4 neurons tested.

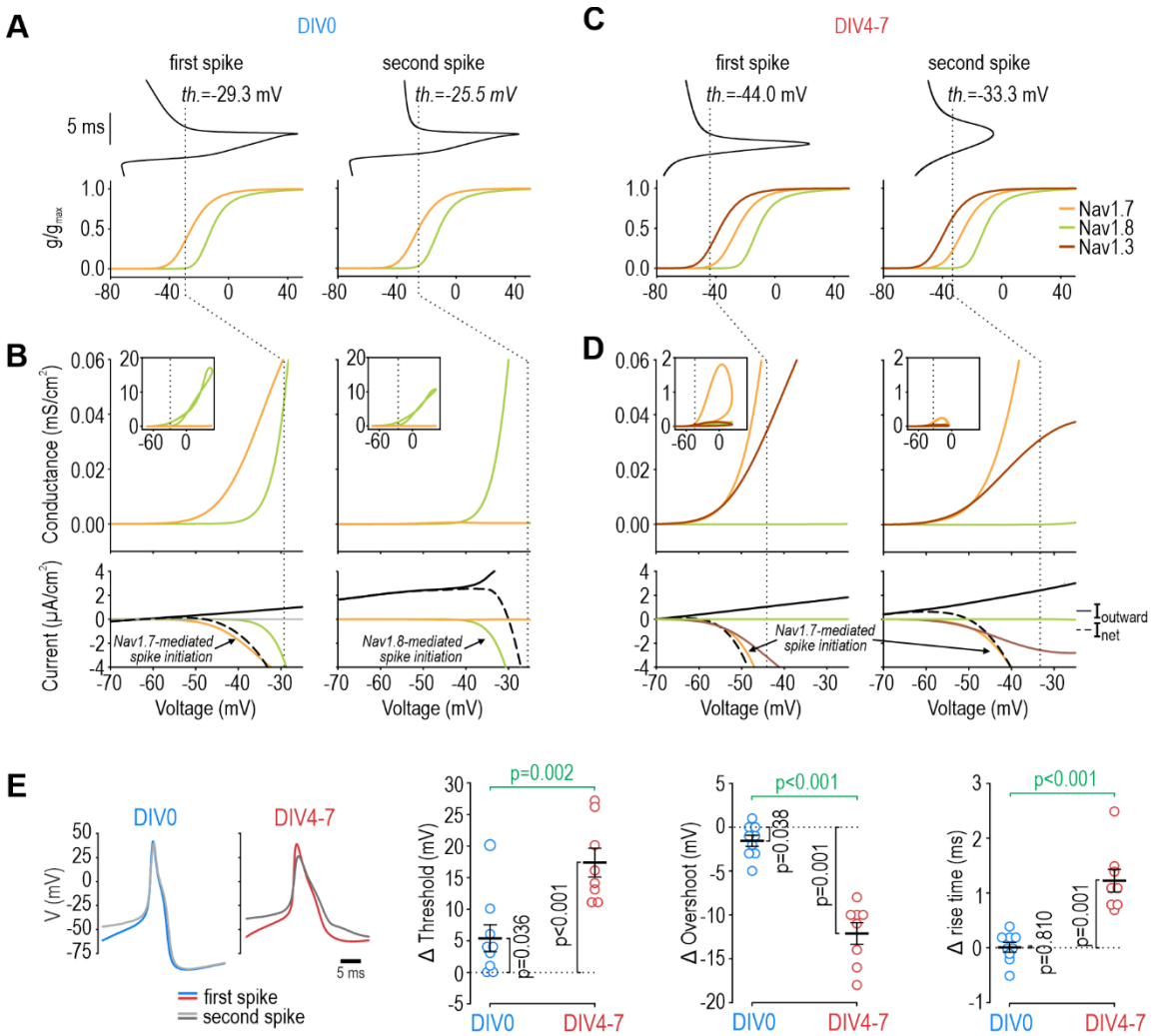

Figure 5. Contribution of $Na_V1.7$ and $Na_V1.8$ to spike initiation in DIV0 and DIV4-7 neurons.

(A) Voltage (top) for first (left) and second (right) spikes in the DIV0 model aligned with voltage activation curves for each Na_V subtype (bottom). Dashed line shows voltage threshold (defined as V where dV/dt reaches 5 mV/ms). **(B)** Conductance plotted against voltage to create a phase portrait (top) showing Na_V conductance at different phases of the spike. Inset shows full voltage range; main graph zooms in on voltages near threshold. Bottom plots show current plotted over the same voltage range. Whereas $Na_V1.7$ (orange) mediated nearly all perithreshold inward current for the first spike, voltage threshold increased – because $Na_V1.7$ inactivated (Fig. 5 – figure supplement 1) – and $Na_V1.8$ (green) mediated nearly all perithreshold inward current for the second spike. The unexpected contribution of $Na_V1.7$ to the first spike correctly predicted that TTX increases voltage threshold in DIV0 neurons (Fig. 5 – figure supplement 2). (**C, D**) In the DIV4-7 model, $Na_V1.7$ (orange) and $Na_V1.3$ (maroon) contributed to initiation of all spikes whereas the contribution of $Na_V1.8$ was negligible (due entirely to its low expression level). **(E)** Sample experimental traces showing differences in the first (blue/red) and second (grey) spikes at DIV0 and DIV4-7. Plots summarize differences (Δ) in threshold, overshoot potential, and spike rise time between 1st and 2nd spikes

during repetitive spiking evoked by current injection. At DIV0, the 1st and 2nd spikes differ significantly in their threshold (T_8=2.522, p=0.036, one-sample t-test) and overshoot (T_8=0.038, p=0.038) but not rise time (T_8=0.249, p=0.810). At DIV4-7, the 1st and 2nd spikes differ in all measures (threshold: T_7=7.613, p<0.001; overshoot: T_7=-9.849, p<0.001; rise time: T_7=5.979, p<0.001). Statistical results (green) show that differences between 1st and 2nd spike at DIV4-7 are significantly larger than differences at DIV0 (threshold: T_{15}=-3.847, p=0.002; overshoot: T_{15}=7.922, p<0.001; rise time: T_{15}=-5.617, p<0.001, unpaired t-tests), consistent with our computational model.

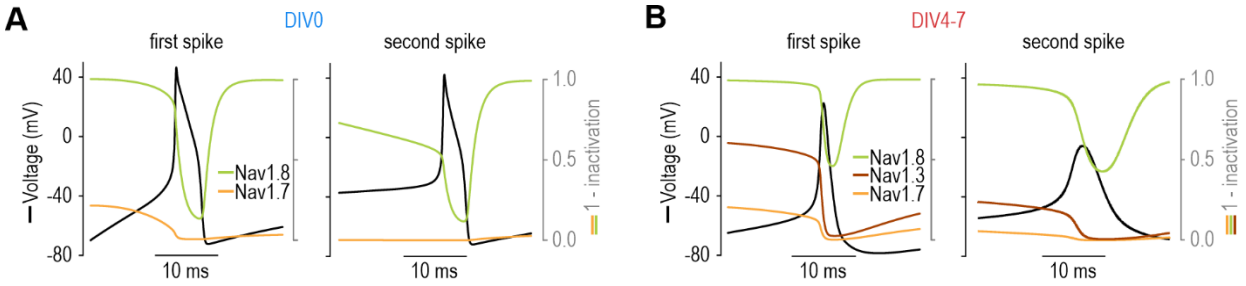

Figure 5 – figure supplement 1. Channel inactivation affects Na_V subtype contribution on short timescale. **(A)** In the DIV0 model, $Na_V1.7$ contributed to the first spike but its inactivation meant that all subsequent spikes relied exclusively on $Na_V1.8$. **(B)** In the DIV4-7 model, despite some inactivation of $Na_V1.3$ (maroon) and $Na_V1.7$ (orange), the remaining current was still large enough (because of the higher g_{max} of those two subtypes) to produce inward current sufficient to support repetitive spiking despite the low g_{max} of $Na_V1.8$ in the DIV4-7 model.

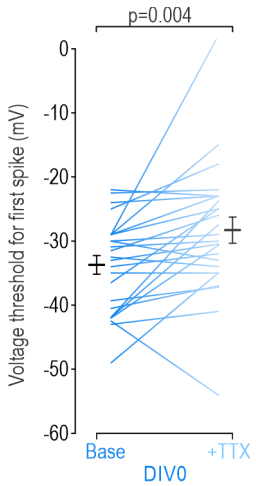

Figure 5 – figure supplement 2. Effect of TTX on voltage threshold in DIV0 neurons.

Despite TTX having negligible effects in DIV0 neurons according to our initial analysis (see Fig. 1), simulation results in Fig. 5A,B predicted that the first spike was nonetheless initiated by $Na_V1.7$. By extension, this predicted that TTX should cause a depolarizing shift in voltage threshold for the first spike. Analysis of the experimental data confirmed this to be true, with threshold (mean±SEM) increasing from -33.7±1.4 mV at baseline to -28.3±1.4 mV after TTX (T_{24}=-3.19, p=0.004, paired t-test). Confirmation of this unexpected prediction helps further validate our model neuron.

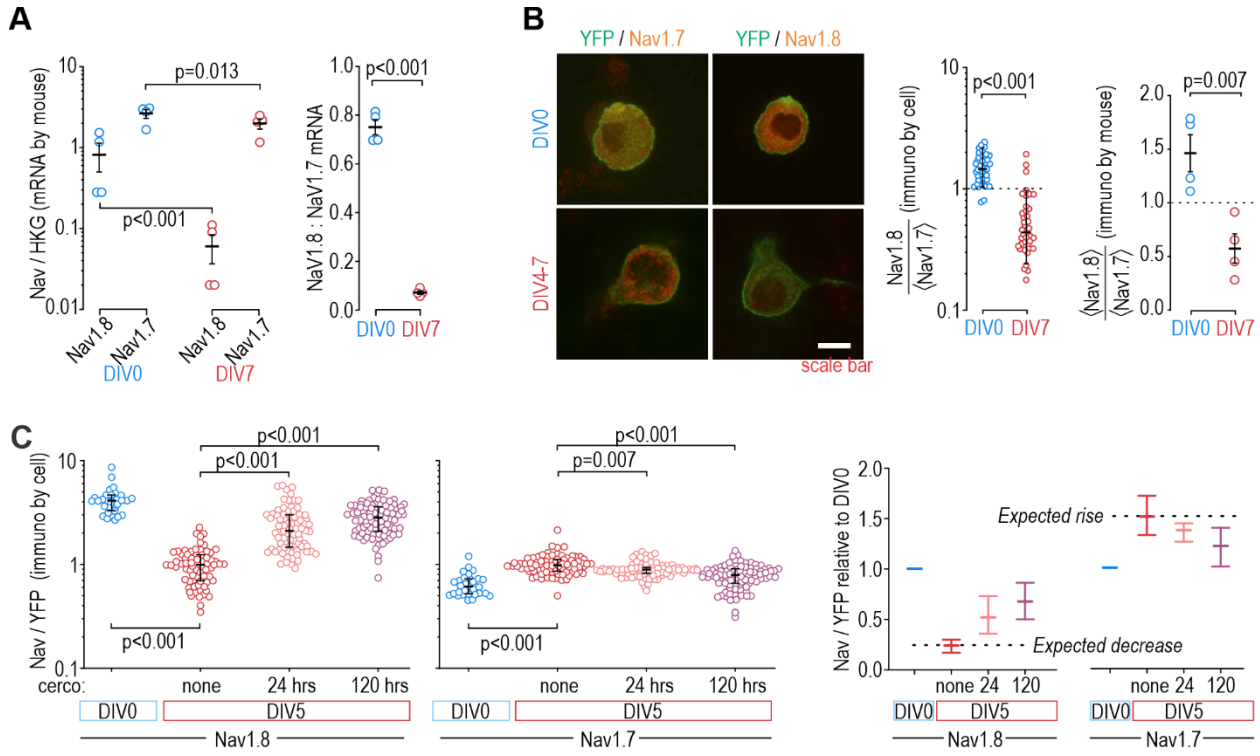

Figure 6. Protein levels, but not mRNA, reflect functional contributions of Na_V subtypes at DIV0 and DIV7. **(A)** Both $Na_V1.8$ and $Na_V1.7$ mRNA levels (relative to a housekeeping gene (HKG), see Methods) decreased significantly between DIV0 and DIV4-7 (factor 1: time, $F_{1,12}$=56.677, p<0.001, factor 2: subtype, $F_{1,12}$=17.952, p=0.001, two-way ANOVA and Student-Newman-Keuls post-hoc tests on log transformed data, n=4 mice per time point) but more so for $Na_V1.8$ than for $Na_V1.7$ (interaction: time x subtype, $F_{1,12}$= 11.455, p=0.005). The differential reduction yielded a significantly higher $Na_V1.8$: $Na_V1.7$ ratio at DIV0 than at DIV7 (T_6=21.375, p<0.001, unpaired t-test) but the increasing functional contribution of $Na_V1.7$ between DIV0 and DIV4-7 remains unaccounted for. **(B)** Immunoreactivity (IR) for $Na_V1.8$ protein exceeded $Na_V1.7$-IR at DIV0, but the opposite was true on DIV4-7, consistent with the functional contribution of each subtype. Na_V-IR was measured relative to YFP intensity in the same cell, and then each cell's $Na_V1.8$:YFP ratio was considered relative to the average $Na_V1.7$:YFP ratio in the co-processed coverslip (left) or average $Na_V1.8$:YFP ratio was considered relative to the average $Na_V1.7$:YFP ratio in the same animal (right). Ratios were >1 at DIV0 but decreased significantly at DIV4-7 (U=78, p<0.001, n=37 for DIV0, n=40 for DIV4-7, Mann-Whitney test (left) and T_6=4.046, p=0.007, unpaired t-test (right)). **(C)** Chronically applied cercosporamide (10 µM) mitigated changes in $Na_V1.8$- and $Na_V1.7$-IR at DIV5 ($Na_V1.8$: H_3=157.95, p<0.001; $Na_V1.7$: H_3=80.662, p<0.001; One-way ANOVA on ranks, Dunn's post-hoc tests, p<0.05 for all pairs). Data are summarized as median±quartile. Panel on the right shows data normalized to baseline (DIV0) to emphasize relative changes. N = 3 experiments.

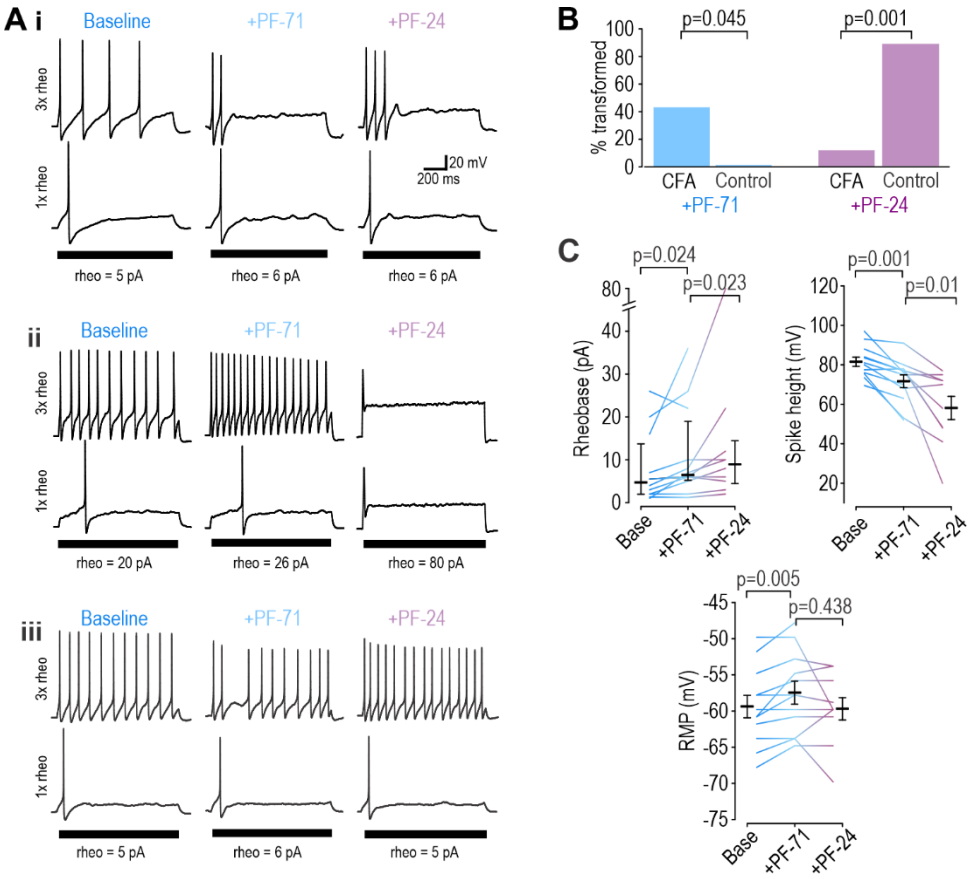

Figure 7. Inflammation alters Na_V subtype contribution to nociceptor excitability.

(**A**) Sample responses in DIV0 neurons from mice injected with CFA three days earlier. In 12 cells tested, PF-71 converted 5 neurons to transient spiking (**i**), encouraged repetitive spiking in 4 neurons (**ii**), and had no effect in 3 neurons (**iii**), thus highlighting increased heterogeneity after CFA. (**B**) At DIV0, the effect of PF-71 differed significantly between CFA and control neurons, converting 42% (5 of 12) CFA neurons from repetitive to transient spiking vs 0% (0 of 9) control neurons (p=0.0451, Fisher Exact test)**.** Applying PF-24 to neurons that continued to spike repetitively after PF-71 had little effect on CFA neurons, converting only 13% (1 of 7) of CFA neurons vs 88% (7 of 8) of control neurons (p=0.001, Fisher Exact test). Together these results argue that $Na_V1.7$ contributes more and $Na_V1.8$ contributes less to nociceptor excitability after inflammation. **(C)** At DIV0, PF-71 significantly increased resting membrane potential (T_{11}=-3.530, p=0.005, paired t-test) and rheobase (Z_{11}=2.186, p=0.024, Wilcoxon rank test), and significantly decreased spike height (T_{11}=4.413, p=0.001, paired t-test) in CFA neurons. Further addition of PF-24 significantly changed rheobase (Z_9=2.176, p=0.023, Wilcoxon rank test) and spike height (T_9=3.237, p=0.01, paired t-test) but did not affect resting membrane potential (T_9=1.049, p=0.321, paired t-test).

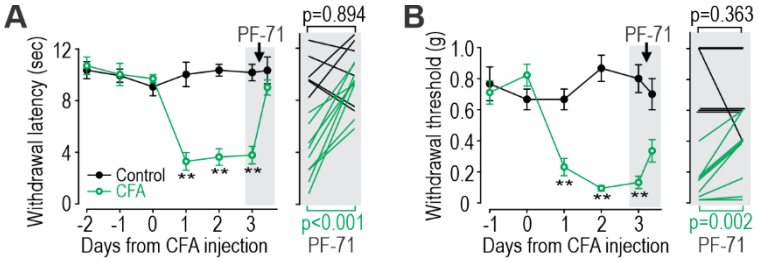

Figure 8. Inflammation-induced change in Na_V subtype contribution impacts analgesic efficacy of PF-71. **(A)** CFA significantly increased thermal sensitivity ($F_{5,65}$=19.556, p<0.001, two-way RM ANOVA). PF-71 significantly decreased thermal sensitivity in mice injected three days prior with CFA (T_8=-7.296, p<0.001; paired t-test) but had no effect in naïve mice (T_5=-0.141, p=0.894). **(B)** CFA significantly increased mechanical sensitivity ($F_{4,52}$=16.786, p<0.001). PF-71 significantly decreased tactile sensitivity in mice injected three days prior with CFA (T_8=-4.341, p=0.002) but had no effect in naive mice (T_5=1.000, p=0.363). Insets in both panels show values for each animal before and 2 hours after PF-71 injection. *, p<0.05; **, p<0.01; Student-Newman-Keuls post-hoc tests.

Supplementary Table 1. Model data before and after channel "inhibition"

	DIV0		DIV4-7		
	Baseline	↓$Na_V1.8$	Baseline	↓$Na_V1.7$	↓$Na_V1.3$
Rheobase (pA)	17	22	12	16	21
Spike height (mV)	72.8	46.9	57.1	21.4	52
RMP (mV)	-69.0	-69.7	-70.0	-69.8	-70.4

Supplementary Table 2. Reagents

Reagent	Description	Source
TTX	Tetrodotoxin citrate	Alomone
PF-24	PF-01247324	Sigma
PF-71	PF-05089771	Alomone
ICA	ICA-121431	Tocris
Papain	Papain lyophilized power	Worthington
Collagenase	Collagenase type II	Worthington
Dispase II	Dispase type II	Sigma

Supplementary Table 3. EC50 values

Drug (concentration used)	EC50 values			References
	$Na_V1.3$	**$Na_V1.7$**	**$Na_V1.8$**	
TTX (100 nM)	**4 nM**	**2 nM**	46±10 μM	(21, 96)
ICA-121431 (1 μM)	**20 nM**	>10 μM	>10 μM	(53)
PF05089771 (30 nM)	11 μM	**11 nM**	>10 μM	(40)
PF-01247324 (1 μM)	>30 μM	>30 μM	**331 nM**	(50)
A-803467 (1 μM)	2.5 μM	6.7 μM	**8 nM**	(97)

Bolded entries indicate the Na_V subtype that is selectively blocked

Supplementary Table 4. Primers

	HPRT	$Na_V1.7$	$Na_V1.8$
NCBI Reference Sequence	*NM_013556.2*	*NM_001290674.1*	*NM_001205321.1*
Length	144	114	148
Forward	TCCTCCTCAGACCGCTTT	TGATGGTCATGGTGATTGGG	AGCCATCAAAGTGTCCGTC
Reverse	TTTTCCAAATCCTCGGCATAATG	TGTTTGCGTCGGTGTCTTC	CTTTATCAGAGCCTCGAAGGTG

Supplementary Table 5. Model equations

Channel Model	Equations
$Na_V1.7$ (86)	$I_{NaV1.7} = \bar{g}_{NaV1.7} m^3 h (V - E_{Na})$ $\dot{m} = \alpha_m(1-m) - m\beta_m$ $\quad$ $\dot{h} = \alpha_h(1-h) - h\beta_h$ $\alpha_m = 10.22 - \frac{10.22}{1+\exp\left(\frac{V+7.19}{15.43}\right)}$ $\quad$ $\alpha_h = \frac{0.0744}{1+\exp\left(\frac{V+99.76}{11.07}\right)}$ $\beta_m = \frac{23.76}{1+\exp\left(\frac{V+70.37}{14.53}\right)}$ $\quad$ $\beta_h = 2.54 - \frac{2.54}{1+\exp\left(\frac{V+7.8}{10.68}\right)}$
$Na_V1.3$*	$I_{NaV1.3} = \bar{g}_{NaV1.3} m^3 h (V - E_{Na})$ $\dot{m} = \alpha_m(1-m) - m\beta_m$ $\quad$ $\dot{h} = \alpha_h(1-h) - h\beta_h$ $\alpha_m = 10.22 - \frac{10.22}{1+\exp\left(\frac{V+7.19+12}{15.43}\right)}$ $\quad$ $\alpha_h = \frac{0.0744}{1+\exp\left(\frac{V+99.76}{11.07}\right)}$ $\beta_m = \frac{23.76}{1+\exp\left(\frac{V+70.37+12}{14.53}\right)}$ $\quad$ $\beta_h = 2.54 - \frac{2.54}{1+\exp\left(\frac{V+7.8}{10.68}\right)}$
$Na_V1.8$ (87)	$I_{NaV1.8} = \bar{g}_{NaV1.8} m^3 h (V - E_{Na})$ $\dot{m} = \alpha_m(1-m) - m\beta_m$ $\quad$ $\dot{h} = \alpha_h(1-h) - h\beta_h$ $\alpha_m = 7.21 - \frac{7.21}{1+\exp\left(\frac{V-0.063}{7.86}\right)}$ $\quad$ $\alpha_h = 0.003 + \frac{1.63}{1+\exp\left(\frac{V+68.5}{10.01}\right)}$ $\beta_m = \frac{7.4}{1+\exp\left(\frac{V+53.06}{19.34}\right)}$ $\quad$ $\beta_h = 0.81 - \frac{0.81}{1+\exp\left(\frac{V-11.44}{13.12}\right)}$
K_M (88)	$I_{KM} = \bar{g}_{KM} n (V - E_K)$ $\dot{n} = \frac{n_\infty - n}{\tau_n}$ $n_\infty = \frac{1000}{1+e^{-\frac{V+35}{5}}}$ $\quad$ $\tau_n = \frac{1000}{3.3e^{V+\frac{35}{10}} + e^{-\frac{V+35}{10}}}$
K_{dr} (88)	$I_{KA} = \bar{g}_{KA} n^3 l (V - E_K)$ $\dot{n} = \alpha_m(1-m) - m\beta_m$ $\quad$ $\dot{l} = \alpha_h(1-h) - h\beta_h$ $\alpha_n = \frac{e^{(-5\times10^{-3}\cdot(V+32)\cdot 9.648\times10^4)}}{2562.35}$ $\quad$ $\alpha_l = \frac{e^{(2\times10^{-3}\cdot(V+61)\cdot 9.648\times10^4)}}{2562.35}$ $\beta_n = \frac{e^{(-2\times10^{-3}\cdot(V+32)\cdot 9.648\times10^4)}}{2562.35}$ $\quad$ $\beta_l = \frac{e^{(-2\times10^{-3}\cdot(V+32)\cdot 9.648\times10^4)}}{2562.35}$
AHP**	$I_{AHP} = \bar{g}_{AHP} z (V - E_K)$ $\quad$ $\dot{z} = \frac{1}{1+e^{5-V/4}} - \frac{z}{100}$

* Modified from $Na_V1.7$: a hyperpolarizing shift of 12mV in V1/2 of activation gate, m

** Modified from (49)

Note that the $Na_V1.7$ and $Na_V1.8$ equations above do not include the liquid junction potential correction of 4.2 mV (86) and 5.3 mV (87), respectively, that were applied in the neuron model.

Supplementary Table 6. Conductance densities at baseline for DIV 0 and 4-7 models

	Conductance densities at baseline (mS/cm^2)						
	$\bar{g}_{\mathbf{Nav1.3}}$	$\bar{g}_{\mathbf{Nav1.7}}$	$\bar{g}_{\mathbf{Nav1.8}}$	$\bar{g}_{\mathbf{Kdr}}$	$\bar{g}_{\mathbf{M}}$	$\bar{g}_{\mathbf{AHP}}$	$\bar{g}_{\mathbf{Leak}}$
DIV 0	0	3	30	3	0.05	3.5	0.025
DIV 7	0.35	35	0.2	3.5	0.5	2.5	0.035